NATIONAL UNIVERSITY OF SCIENCE AND TECHNOLOGY POLITEHNICA BUCHAREST

Doctoral School of Electronics, Telecommunications and Information Technology

Decision no. 205 from 21-09-2024

PHD THESIS SUMMARY

Eng. Matei-Constantin ȘERBĂNESCU

PORTABLE DATA ACQUISITION AND CONDITIONING SYSTEMS FOR IOT APPLICATIONS

DOCTORAL COMMITTEE

Prof. Dr. Ion MARGHESCU Univ. Politehnica of Bucharest	President
Prof. Dr. Gheorghe BREZEANU Univ. Politehnica of Bucharest	Supervisor
Prof. Dr. Marina ȚOPA Univ. Tehnica of Cluj-Napoca	Reviewer
Lect. Dr. Gheorghe PRISTAVU Univ. Politehnica of Bucharest	Reviewer
Dr. Octavian BUIU IMT Bucharest	Reviewer

BUCHAREST 2024

Contents

Chapter 1

Introduction

1.1 PhD thesis domain outline

The Internet of Things (IoT) concept emerged from the people widespread need to access information from various sources, pointing towards diverse things such as weather data, medical data, velocity data, position data, data concerning industrial processes, etc. Essentially, IoT promotes new ways of communication between people, people and things, but also between things. This fact contributes significantly to the globalization process, launching into discussion a third dimension in the informational world – that of a "thing". Currently, the IoT concept makes its presence felt in traditional domains such as medicine or agriculture, while also being an important driver in the development of new applications, for instance urban traffic management or the digitalization of large factories. Specifically, among the means by which IoT contributions stand out is the interconnection of dozens (hundreds in some cases) of portable and intelligent acquisition and conditioning systems, ensuring data convergence (temperature, humidity, pressure, etc.) in order to facilitate a decision-making process. A sensor system can be regarded as *intelligent* when the signal acquired from the sensitive element is conditioned by filtering and amplification circuits, converted into digital format and transmitted by various methods to a beneficiary. This can either be a human operator or another electronic equipment. Clear requirements in terms of energy efficiency, production costs, autonomous operation, low complexity or data security have been formulated for such systems.

1.2 PhD thesis purpose

In line with the facts presented in the afore paragraph, the doctoral thesis subscribes to the field of portable and intelligent sensor systems with applicability in the medical, agriculture or consumer electronics fields. The main objectives of this work are the conception, design, practical implementation and experimental validation of two sensor systems proposed for

temperature or humidity measurements, adhering to the current IoT requirements. With respect to the order in which they appear in the doctoral thesis, the first one addresses the segment of medical equipment used to investigate diabetes complications. In this regard, a solution for monitoring the temperature of the plantar areas is proposed, the purpose of which is to prevent the occurrence of ulcers formed in the early stages of the diabetic foot pathology. The presented solution boasts modularity and portability, featuring a temperature sensor module, as key element. The module offers a degree of novelty in terms of the flexibility in moving the measurement points of interest on the plantar surface and the possibility of accessing real time temperature data, collected from the affected areas. The second measurement system developed in the doctoral thesis targets chemoresistive humidity sensors obtained from innovative nanocarbon materials. The system is based on the premise that the performance demonstrated by a resistive sensor can be equally attributed to the sensitive material and its acquisition and conditioning circuit. The principle proposed for signal-conditioning involves the conversion of the sensor resistive gradient into a rectangular signal with variable duty-cycle.

1.3 PhD thesis contents

The doctoral thesis is structured in three chapters, to which Introduction and Conclusions are added. *Chapter 2* follows the Introduction and contextualizes the subject of the thesis, extensively discussing fields of application and Internet of Things exigencies.

Chapter 3 will be dedicated to a plantar temperature monitoring system for a diabetic patient, with immediate applicability in preventing the onset of typical diabetic foot ulcers. The presentation begins with the purpose and necessity of a system of this kind, for the prevention of complications brought by diabetes, targeting the aforementioned pathology. A system prototype, consisting of 8 modules with temperature sensors, connected to an acquisition board, is practically implemented at a printed circuit board (PCB) level. The goal is to highlight several performance markers, such as measurement resolution, sensor modules response time or the average consumption in active acquisition mode.

Chapter 4 presents a signal-conditioning system from chemoresistive humidity sensors, with potential use in the assessment of air quality in residential areas or greenhouses. By exposure to humid conditions, the base resistances of these sensors vary, in different degrees, from hundreds of Ωs to a few kΩs. The proposed readout principle will be outlined and backed by the two implemented system prototypes – one for resistive elements with moderate swings and another one, optimized, for complete resistive swings.

Conclusions chapter makes an incursion through the results of this work, the original contributions, as well as the list of scientific papers published during doctoral studies. The closing remarks offer future development prospects with respect to each system.

Chapter 2

Sensors for IoT

2.1 Internet of Things

The influence that information and communication technologies have on daily activities plays a decisive role in the development of a modern and sustainable society. The evolution of Internet of Things begins in the 1990s, when research studies concerning automation processes or systems' computing power increase (meant to cope with a continuous flow of information) became prominent in scientific literature. In essence, the authors' vision leaned towards a standard and clear way in which computers understand the real world [1], [2]. The development of modern web search engines, together with the large-scale digitalization of production processes from various industries provided a solid foundation in terms of connecting people and objects. Later, the spread of portable and affordable computer systems such as smart mobile phones or tablets, as well as social networks, made it possible for the population to interact continuously [3]. At present, IoT applications have penetrated areas such as telemedicine, agriculture, urban traffic management, electricity distribution or fitness (i.e., physical activity to maintain the human body).

The IoT vision proposes to complement existing capabilities through a consistent interaction between a wide range of electronic systems/applications, controlled completely, partially or not at all by a human operator, at a specified moment in time. In a collective sense, the definition of a connected system relies on preserving the functionality for which it was designed, while referring to its access to an Internet network, through which it can be controlled remotely. For instance, the use of a smart fitness bracelet becomes relevant only when it's connected to a mobile application, allowing the user for easy access to heart rate measurements or burnt calories. As such, it can be stated that an IoT ecosystem can be completely characterized by three components, as follows: data measured and stored locally, a processing algorithm and a software application installed on a computer system (it can be a smartphone or a tablet), for fast user integration. The current challenges associated with smart sensor systems refer to stimuli response time improvement, streamlining consumption and development costs, ensuring data security, as well as the adoption of new sensing materials that lower the pressure on traditional ones [4]–[7].

2.2 Sensors - Overview

2.2.1 Definition

Over the course of time, sensors accompanied and assisted humanity in activities such as analysis, monitoring, warning and control for the aeronautics, military, automotive and, more recently, medical systems industries. The etymology of the word *sensor* refers to the reception of a physical, chemical or biological stimulus and the transmission of the resulting electrical impulse. Essentially, it can be stated that the sensor makes a translation between a non-electrical and an electrical quantity, leading to the generation of an output signal that can be a current, a voltage or an electric charge. Nowadays, that signal is taken over and conditioned by filtering or amplification circuits and transmitted by various methods to a beneficiary. This can either be a human operator or another electronic equipment that simplifies a decision-making process. Essentially, this is what gives the *smart* attribute to a modern sensor system.

As sensor systems reach new levels of miniaturization and intelligence, they're also developing expanded data collection capabilities, finding additional areas of use as compared to traditional ones. In general, price, performance and size have been considered as the main factors in the development of new sensor technologies, but aspects such as the sensing material used, energy-efficiency or the way of transferring data have gained the same importance in recent years.

2.2.2 Applications

Historically, the steam engine, electricity, industrial processes automation, the transistor and integrated circuits advent, as well as the widespread use of complex computer systems have contributed one by one to the industrial revolutions that humanity witnessed until the dawn of the twenty-first century. Behind these remarkable advances was actually the need to simplify production processes, reduce human effort, increase precision or work speed. The modern information society is building upon these advances, and another industrial revolution is synonymous with new branches such as autonomous cars, robotic surgery and digital factories. At the same time, it can also be associated with concepts such as the Internet of Things, Artificial Intelligence or Machine Learning processes. Sensors are a common element amongst all these, placing themselves at the very bottom of the information pyramid.

The doctoral thesis analyzed two areas in which sensors are often used: the automotive industry and the medical field. The former has seen a significant increase in the demand for sensors, in the context of severe rules to limit carbon emissions, the accelerated

adoption of driver assistance systems [8] and autonomous driving or the demand for electric vehicles. In this regard, the use of sensors can also be extrapolated to the concept of Intelligent Transportation System [9], which relies to a great extent on the platforms used to collect and process data on road infrastructure and traffic conditions. Sensors have become an integral part of a modern road transportation infrastructure, providing the information needed to outline a complete picture of traffic conditions, with data about: speed, gauge and number of vehicles, lane occupancy, road condition (humidity, unevenness, etc.) [9].

Medical applications are the second area referred to in the thesis in terms of the usage of sensors, including as being an integral part of an Internet of Things ecosystem. Advances in portability, the miniaturization of sensitive devices and associated measurement circuits or new ways of transferring and harvesting energy have led to a mutual influence between medicine and smart sensor systems. Essentially, they broaden the horizon of detection and prevention methods in case of a severe medical condition (e.g., diabetes, cardiovascular diseases or cancer), while also facilitating remote monitoring of patients with mild chronic conditions or during physical rehabilitation processes. The following list provides a landscape of medical applications for which sensors became essential in recent years [10]–[12]: evaluation of vital signs, monitoring of disease stages, medication's controlled administration, remote patients' evaluation, endoscopic and laparoscopic surgery, rapid medical evaluation at the point of care, environmental conditions evaluation from a medical room.

Moreover, the doctoral thesis presents in a great level of detail the ways of classifying sensors according to the detection mechanism and the passive or active character of the sensitive element, as well as the main characteristics, which contribute to the designer's decision to use a given sensor in a specific application.

2.3 Resistive sensors

The success of resistive sensors is largely due to their availability for a wide range of practical applications, such as: thermal or light detection, evaluation of humidity, gas concentration, measurement of position or mechanical deformation, etc. In respect to the operating principle, a resistive sensor provides information based on changes in electrical resistivity, ρ of a material or electrical resistance, R of a device, subjected to a physical, chemical or biological stimulus. Electrical resistivity is represented by the opposition that a material imposes on the charge carriers when an electric field is applied. Therefore, this is the subject of a microscopic phenomenon. This makes the estimation of electrical resistivity difficult to achieve with the usual methods involved in the development of

electronic measurement systems. By contrast, electrical resistance is a property assigned to a component with a well-established shape and size, which makes it easier to measure.

Ohm's law provides a precise relationship between the voltage applied to a device and the current flowing through it, being one of the basic techniques in determining electrical resistance. Moreover, if that device is made of a homogeneous material, then its geometric characteristics, together with the resistivity of the material, can lead to obtaining R. However, Ohm's law, in its classical form, is no longer valid if the sensor has also capacitive or inductive elements, while being biased with a current or voltage that varies over time. In these cases, the notion of sensor impedance comes into play, and the measurement circuit used must evaluate both its real and imaginary parts, at the same time.

According to the principle of operation and based on the stimuli to which they respond, there are several types of resistive sensors, as follows: chemoresistive, piezoresistive, magnetoresistive, photoresistive, temperature-resistive or bioresistive. The first category is the subject of one of the applications presented in the doctoral thesis and is discussed in detail in a later chapter [13], [14], [15].

In a practical IoT application, in order to correctly and completely provide the desired information, a sensor can be accompanied by both an analog block for acquiring and conditioning its signal and a digital one for storage and processing (e.g., a microcontroller). When the electrical signal from the sensor's output is generated, it may contain unwanted components, requiring filtering, or it may have a very low amplitude (on the order of a few mV or μA), requiring amplification. Equally, for modern sensors, designed at the integrated circuit level, the format of the digital output signal is an aspect that must be taken into account for the adequacy of the communication interfaces available in that system. Figure 2.1 shows, in a simplified manner, the path taken by the sensor signal, from the application of the stimulus to the delivery of the desired information in the system.

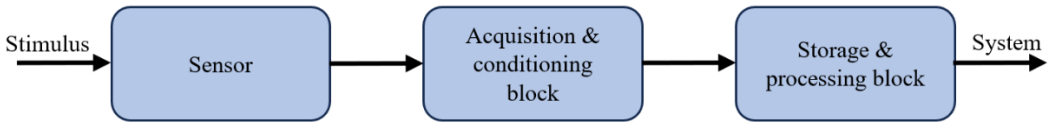

Figure 2.1 *The generic path taken by the signal coming from a sensor to the delivery of the desired measurement information in a given system*

The representation degree of the input stimulus in the output electrical signal can be judged either on the basis of a general set of characteristics or particularly, according to the specific accuracy and reliability requirements of the given application. Distortions visible on this signal can be random or systematic. The latter are generally correlated with design errors, material quality, production tolerances or non-compliance with a calibration procedure. However, random disturbances are difficult to quantify and can be caused by any electronic equipment in the vicinity of the sensor system, including radio interference or noise from the power supply. Therefore, for the correct design of the circuits that follow the sensor, understanding the noise sources and parasitic elements is essential. A high-performance

measurement system must highlight the useful signal coming from it, attenuating noise as much as possible.

2.4 Acquisition and conditioning systems for resistive sensors – State of the art

The race to develop smart sensor systems is influenced by the growing popularity of the Internet of Things concept, which brings to the fore not only opportunities and new applications, but also numerous demands. The positioning of the resistive sensors in this context underlined the fact that the expectations related to their performance can be equally associated with both the sensitive material used and the signal conditioning circuit. Following a literature inspection, the doctoral thesis extensively presents measurement solutions designed as complex integrated circuits or based on discrete components and implemented on a printed circuit board (PCB). This section summarizes works published in the last 5 years, where techniques for acquiring and conditioning signals from various sensors (gas, pressure, etc.) are proposed, regardless of their resistive excursion.

In IoT applications, the reduced complexity and efficiency of the area occupied on a PCB by a Application Specific Integrated Circuit (ASIC), used in conjunction with a digital data processing and transmission unit, have led to research in the field of transconductance amplifiers, instrumentation amplifiers and Σ-Δ modulators, as essential building blocks of such an ASIC. Although the use of an ASIC contributes significantly to reducing the complexity of measurement systems, the practical implementation of an integrated circuit often reveals prohibitive costs even for series production, at odds with the requirements and specifics of IoT applications. As for measurement systems made with discrete components, there are authors who still prefer to place the sensor in a Wheatstone bridge configuration. Obtaining four perfectly paired sensing elements to achieve a linear bridge response is a difficult challenge, so efforts are often focused on linearizing half-bridge or quarter-bridge structures. In this regard, various methods have been proposed in literature to improve the linearity of these configurations' output voltage curves [16]–[20].

Following the literature synthesis, the current challenges were highlighted: robustness, consumption efficiency and production cost and increasing the dynamic range from the output of these systems, in order to fit the IoT requirements. Regarding the system architecture, in addition to the signal acquisition and conditioning circuit, the need to complete it with the following functional blocks is reiterated: microcontroller, power supply block, communication block. Each of these blocks has a well-established role in the economy of a modern intelligent sensor system, these aspects being extensively commented in the thesis.

Chapter 3

Temperature sensors for IoT medical applications

This chapter presents an innovative system architecture for a modular plantar areas temperature monitoring solution, with applicability in the prevention of diabetic foot pathology. Ulcers in the plantar region represent one of the most common complications of diabetes, posing a high risk of lower limbs amputation, which gives this pathology a disabling character. The proposed solution, which can fit into an Internet of Things medical ecosystem, allows for the simultaneous scanning of both plantar areas of a diabetic patient and can lead to an early detection of local inflammations. It consists of two parallel strings of digital temperature sensor modules, serially connected to a main board, which facilitates the acquisition and data transfer to a computer. The proposed concept was validated with the help of a prototype based on 8 measurement modules. The resulting assembly demonstrated a measurement resolution of 0.05 °C, a response time of approximately 60 seconds and showed an average active current consumption of 17 mA.

3.1 IoT in medicine

The current medical ecosystem, adhering to the IoT requirements, entails a transition from the approach centered on the effects' treatment regarding certain medical conditions to one of prevention and reduction of the risks associated with their occurrence. Based on the demonstrated synergy between IoT and smart sensor systems, doctors and engineers can now work together in a collaborative and interdisciplinary framework to hasten the use of modern technologies as instruments for monitoring and analyzing patients' condition. Diabetes, together with its complications represent medical conditions for which the adoption of investigational methods based on temperature or pressure sensor systems is highly recommended [21]–[24]. In literature there are numerous studies, even recent ones, also corroborated with the statistics published by the International Diabetes Federation, which indicate the existence of about 550 million patients with diabetes worldwide [25],

[26]. On top of that, projections for the next decade reflect an increase to more than 700 million people belonging to this category. Although this disease is preventable, its prevalence in low- and middle-income countries makes it difficult to manage due to poor health services.

The Coronavirus pandemic, in its contribution to the decentralization of medical procedures established for diabetic patients, has encouraged research and innovation in the field of portable or wearable sensor systems, aimed at providing independence to the patient and simplifying the interaction with medical personnel. The statistics previously presented make a strong case on the importance of an optimal solution for diabetes management, based on a paradigm shift in the efforts of the scientific community, which must now be oriented towards new, preventive and non-invasive methods of diagnosis and monitoring of its complications. The ability to access sensor data in real time or to create a history log for a certain time interval enhances the understanding that the person suffering from diabetes has of their condition. This also increases the degree of education and accountability regarding compliance with medication and personal care procedures at home. Basically, smart sensor systems provide distributed efficiency in medicine on several levels, from diagnosis to care costs.

3.2 Diabetic foot pathology

Diabetes is a chronic disease inflicted either by the body's inability to handle high blood glucose concentrations or by inadequate insulin production. Among the associated risk factors we may find the hereditary condition, weight in excess, stress, poor diet or lack of regular physical activity. In the absence of early diagnosis and adequate medical treatment, it can lead to various complications, usually affecting the cardiovascular system, kidneys, vision or even motor function through the appearance of diabetic foot ulcers. The latter, commonly known in medical literature under the acronym DFU, represent a disabling category of complications, which, over time, cause infections of the plantar area, leading to lower limbs amputations.

From a medical standpoint, there are two fundamental concurring pathologies in the occurrence of diabetic foot: neuropathy and vasculopathy [27]. The first generally causes a decrease in the sensory capacities associated with pain and temperature and a deterioration of the sweating function in the sole, favoring dry skin and the appearance of cracks. Complementarily, vasculopathy reveals itself as a peripheral arterial problem, which prevents open wounds from healing, also leading to infections in the plantar area. The prevalence of this condition is accentuated in the case of diabetic patients who already suffer from ischemia in the lower limbs. Interest in methods of early DFU diagnosis or investigation has been present in the medical scientific community since the 1970s.

Sandrow *et al.* demonstrated that temperature measurement in the plantar areas of a diabetic patient can help identify local inflammations and thus predict the onset of DFU [28]. Specifically, the comparison of temperature data resulting from the simultaneous monitoring of both plantar areas can assist in the localization of a restricted area where inflammation develops. In this sense, the difference most frequently reported in literature is 2.2 °C [29]. The comparison applies either to the same area on the sole of both feet, or between two areas of the same sole, following monitoring on consecutive days. At the same time, studies show that thermal analysis helps patients to avoid applying high pressure to the areas thus identified, something that can be achieved with the help of customized shoes. However, at present, the procedure of comparing the temperature of the two plantar areas is mainly carried out by specialized personnel in a clinical environment. This fact brings with it the burden of long waiting intervals between appointments and the population's reluctance to interact with doctors or to visit hospitals.

In the following paragraphs, the state of the art concerning electronic systems for the evaluation and monitoring of diabetic foot pathology will be briefly discussed, subsequently followed by the architecture proposed in this PhD thesis.

3.3 Temperature sensors acquisition and conditioning systems for medical applications – State of the art

In this section, the state of the art regarding sensor systems proposed for the investigation of the diabetic foot will be briefly presented. A literature survey was carried out, especially among the works published on this topic in the last 5 years. The identified systems, often integrated into footwear and textile materials (socks with sensors) or presented as platforms that patients can step on, were extensively discussed in the PhD thesis.

In [30], Drăgulinescu *et al.* carried out, in a comprehensive manner, a review of the smart sock sensor systems published up to that point with the aim of investigating medical conditions, gait and locomotion parameters or sports activities. The authors performed a segmentation of the identified systems according to the applications they target, pointing out the benefits that such a system can have for the investigation of DFU. The paper also emphasizes the challenges that researchers in this field face, as follows: the cost of developing a prototype, the precision, the measurement surface covered by the sensors, the number of participants enrolled in the study, the comfort and ergonomics they benefit from, the ways to transfer and the algorithms for the analysis of the experimental data obtained [21]–[25], [31].

Next, a measurement solution that was found in several of the recently published studies is that of a platform that patients could step on for a short, predefined time and that is able to offer a thermal map of the plantar surface [32]–[35]. A notable example, developed by

a company from the United States, is Podimetrics [35]. It is based on a matrix of analog temperature sensors (the total number amounts to 2000), arranged under a thermo-conductive, bacteriostatic and water-resistant coating. Although Podimetrics has been certified for commercial use, it has not yet become widely available. Instead, the product significantly contributed to the promotion of the procedure of monitoring the temperature of the soles simultaneously with a high reccurency (weekly or even daily). Another long reported method in literature and still widely employed is the infrared thermometry. It is considered a cheap and non-invasive way to collect temperature data, being also one of the main methods still used in clinical analysis [36]–[38]. Despite its known simplicity, this method does not offer the desired independence to diabetic patients, as the collection of images must be, all the time, conducted by a doctor, a caregiver or a relative.

In the next sections, the proposal for a modular plantar temperature monitoring system will be presented, details regarding the practical implementation of a measurement prototype will be given and the experimental results obtained with that will be discussed.

3.4 Plantar areas temperature monitoring system

3.4.1 DiaMOND system architecture

Among the main objectives of the PhD thesis are the conception, design and practical implementation of a temperature monitoring system for the plantar area. The purpose of this endeavor is the early detection of the temperature gradient that occurs on the soles in the early stages of the installation of the diabetic foot pathology. As such, the acquisition system must be able to alert the diabetic patient when a temperature difference greater than 2.2 °C is detected between two corresponding points in position on both soles, or even between two regions within the same plantar surface.

The block diagram of the proposed architecture for the DiaMOND system is depicted in Fig. 3.1 [39]. The main board consists of a microcontroller, a Bluetooth Low Energy (BLE) module and a power supply block.

This subsystem is connected to two parallel strings consisting of modules with independent temperature sensors (MS), associated to each plantar region. The MS is an essential element of the architecture shown in Fig. 3.1, which provides the DiaMOND system with modularity.

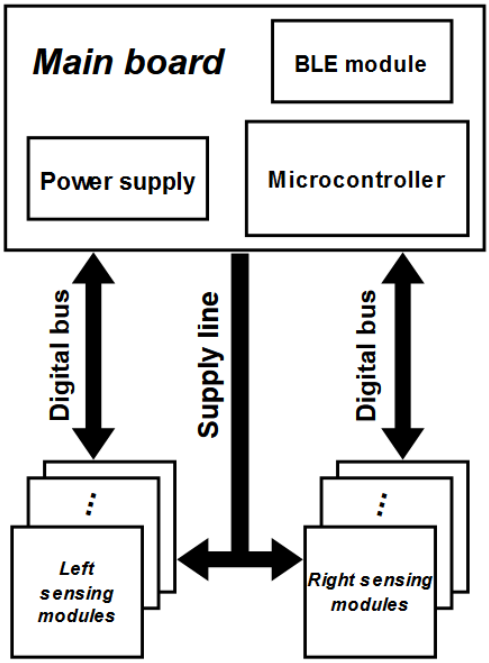

Figure 3.1 *DiaMOND system architecture*

This attribute gives the proposal a degree of novelty distributed on two levels. First, it provides flexibility in moving the measurement points of interest on the plantar surface, depending on the size of each patient's foot. On the same importance level, MS enables the user to access real-time temperature data collected from the soles, a fact which can eventually facilitate the creation of a heat map of the plantar areas.

At the same time, the proposal aims to ensure patient independence by designing DiaMOND as a portable, battery-powered monitoring system. In this regard, it is proposed to use a single voltage domain (VDD), compatible both with the circuits on the main board and with the temperature sensors placed on the MS. Portability is also ensured by the presence of a BLE module. These features allow easy integration of DiaMOND into a medical IoT ecosystem, which would significantly simplify the interaction between the patient and his attending physician.

For the digital communication between the MS strings and the main acquisition board, the I^2C protocol was chosen. It is widely used in portable electronic systems, having the great advantage of a communication through only two signal lines, *Serial Data* - SDA, respectively *Serial Clock* - SCL. Another important feature of the proposed system is the possibility of immediate identification of the sender between the temperature sensor modules, each one boasting a unique digital address. The total number of MSs connected to the I^2C bus can be adjusted according to the physician's requirements or the shape of the patient foot.

3.4.2 DiaMOND practical implementation

For the DiaMOND architecture depicted in Fig. 3.1 a printed circuit board (PCB) level implementation was pursued. As such, a PCB was built for both the motherboard and the MS, individually. The selection of parts took into account their cost, current consumption and the dimensions of each. Also, for the microcontroller and the temperature sensor, the possibility of power supply between 0 V – 3.3 V was considered. Next, the list of the main components used is given:

- Temperature sensor – MAX30205 [40], Analog Devices (part of MS – Fig. 3.1),
- Microcontroller – dsPIC33CK256MP502, Microchip (Fig. 3.1),
- Power supply – synchronous Buck converter MCP1603 [41], Microchip (Fig. 3.1).

MAX30105 is an integrated sensor that provides temperature information in digital form suitable for I^2C communication. It converts the acquired data using an internal Σ-Δ type ADC, having a maximum measurement error of ± 0.3 °C, in the range 15 °C – 36 °C [40]. Remarkably, the sensor provides up to 32 unique I^2C addresses, which theoretically allows chaining of 32 modules (MS – Fig. 3.1) in each string connected to the main board (Fig. 3.1). This can be translated into 32 measurement points spread all over each plantar region. The way I^2C addresses are selected is facilitated by three address terminals, A0, A1, A2. For each terminal there is the possibility of connecting to VDD, GND, SDA, respectively SCL. Table 3.1 shows an example regarding the setting of three distinct addresses, determined by the change of state A0, A1, A2 [40].

Table 3.1 *Example of obtaining three different I^2C addresses for MAX30205*

A0	A1	A2	I^2C address
GND	GND	GND	90h
GND	VDD	GND	94h
VDD	GND	GND	98h

The measurement principle of the MAX30205 involves establishing a strong thermal coupling between the surface to be measured (the sole skin of a diabetic patient) and the exposed pad of the integrated circuit, which communicates directly with the internal sensing element. In the case of the application shown, this was achieved by coupling the exposed pad (using 6 vias) to a 1 cm^2 Copper area on the Bottom layer of the PCB. This surface will be electrically coupled to GND, thus designated as the contact area for temperature measurements. The 6 vias are considered identical and have an inner diameter of 0.4 mm and a height of 1 mm (the height of the MS PCB itself). The via wall thickness was set at 70 μm. The material used for metallization was also Copper. For the proposed system, the thermal resistance of a vine was calculated to be ≈ 25 °C/W. Considering that 6 such structures were clustered on a surface of 2.4 x 1.6 mm^2, the equivalent thermal

resistance can be approximated to 4 °C/W. PCB height and via hole size are two of the parameters that dictate production costs for the sensor modules shown. Figure 3.2 illustrates the PCB obtained for the MS, with an area of 4 cm^2 [39]. The contact area on its Bottom layer is surrounded by a thermal barrier formed by holes (without electrical connection) with diameters between 0.8 mm and 1.5 mm. Apart from the MAX30205 sensor (3 x 3 mm^2), the MS contains only passive components.

To deliver the VDD voltage, a synchronous buck converter, MCP1603 [41], was used, which ensures an output voltage fixed at 3.3 V and can deliver a maximum load of 500 mA. The converter works at an internally fixed switching frequency of 2 MHz. The system input voltage is normally equal to 5 V, and a value of 4.7 µH was calculated for the storage inductor. The input and output capacitors were 10 µF and 4.7 µF, respectively.

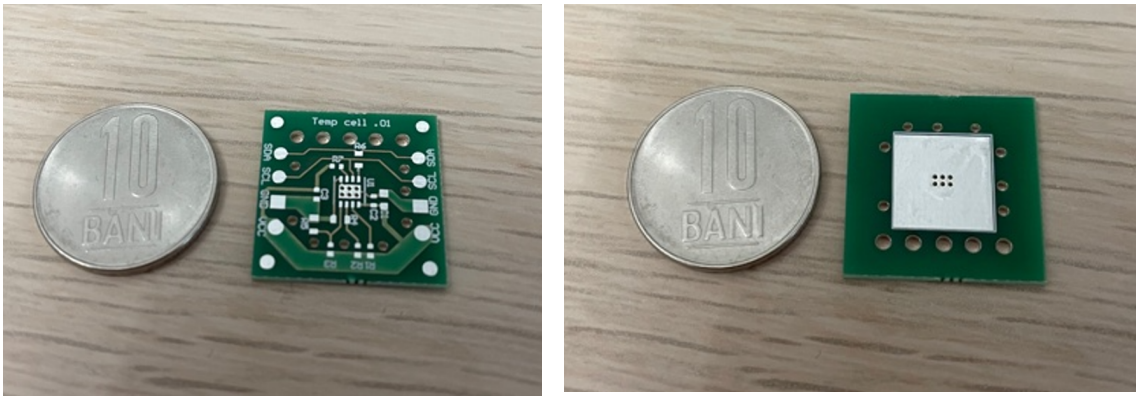

a) ***b)***

Figure 3.2 *PCB of MS: a) Top layer, with MAX30205, b) Bottom layer, with the contact area*

To validate the correct operation of the converter, the voltage ripple of VDD and its stabilization ramp were tested. The measured start-up time is 356 µs, a perfectly monotonic ramp being observed until plateau is reached. The voltage ripple value is 56 mV, which represents < 2% of the nominal value of VDD (3.3 V).

3.4.3 Experimental results

To demonstrate the performance of the DiaMOND system, a prototype was assembled with 8 sensor modules (hereinafter referred to as MS1 – MS8), connected to the main board. The input voltage was kept at 5 V and the sensor acquisition rate was set at 1 sample/second. The connection between the modules was made with four Copper wires, 1 mm in thickness and 2 cm long each. The connection to the main board was provided with the same type of wires, but 6 cm long. The assembled prototype is illustrated in Fig. 3.3.

As a first step, a test was carried out at ambient temperature, without skin contact. This was meant to highlight the accuracy and pairing degree of the 8 modules. The obtained result is presented in Fig. 3.4 [39].

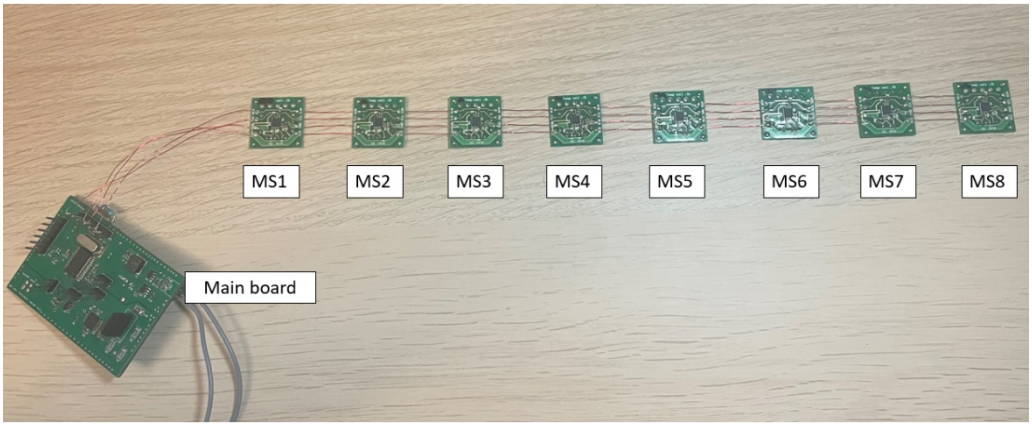

Figure 3.3 *DiaMOND prototype, 8 MS boards serially connected to the main board*

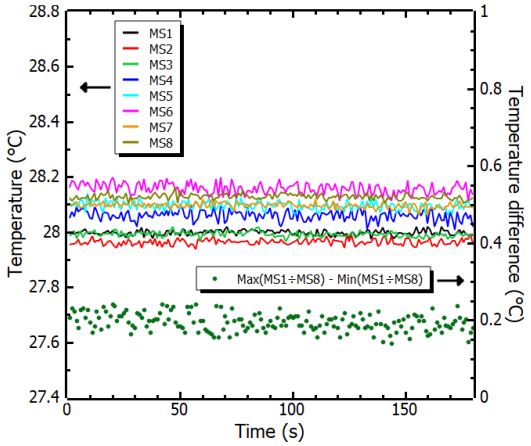

Figure 3.4 *Ambient measuremts, with MS1 – MS8*

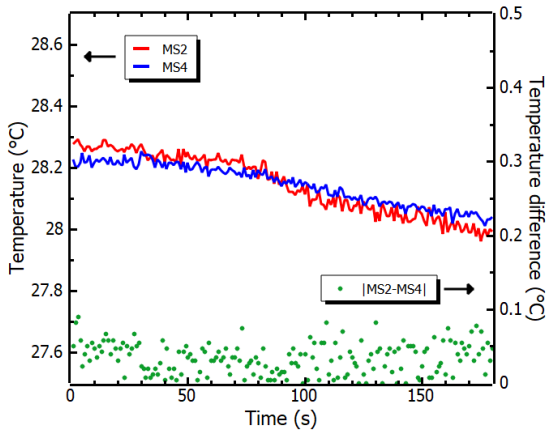

Figure 3.5 *The result of contact areas thermal coupling for MS2 and MS4*

The total acquisition time was three minutes. It can be noted that during all this period, the response of the 8 modules remains similar, falling between 27.9 °C and 28.2 °C. At the same time, the difference between the most disparate points of the 8 curves (green points – Fig. 3.4) was also calculated. In this case, an average value of approximately 0.19 °C resulted. This value can be attributed to natural temperature fluctuations within the room where the test was carried out. As such, a very good uniformity degree can be noted among the 8 assembled sensor modules.

Next, based on the graph shown in Fig. 3.4, two modules, MS2 and MS4, were selected to confirm their pairing by thermally coupling the contact areas of each other. The result of this test is presented in Fig. 3.5. An excellent matching of the values acquired by the two modules can be observed, the average calculated difference being < 0.05 °C (green dots –

Fig. 3.5). As such, the measurement accuracy of the presented prototype plainly covers the performance requirements imposed by the diabetic foot pathology (ΔT exceeding 2.2 °C).

To confirm the performance of the acquisition system in a real use-case, skin contact measurements were also performed. Figure 3.6 shows the result obtained from a three-minute test performed on the plantar skin of a healthy adult, using the MS1 and MS2 modules. The distance of 2 cm between them was maintained. The acquisition system was able to detect a constant temperature difference after only 60 seconds. This is highlighted by the blue curve, which is the local average of 10 consecutive samples from the difference data (MS1-MS2) (green dots – Fig. 3.6). For a healthy adult, this average is < 0.2 °C, but the detection itself of such a small value places guarantees regarding the monitoring of a diabetic foot with the method proposed in this thesis.

Additionally, the response time of the presented prototype was evaluated. Modules MS1 and MS2 were employed again. The first was placed on the forehead and the second on the tip of the index finger. Simultaneously, these two regions were monitored with medical-grade thermometers (T1, T2). The result of this test is given in Fig. 3.7, while Fig. 3.8 shows the temperature difference between the two areas.

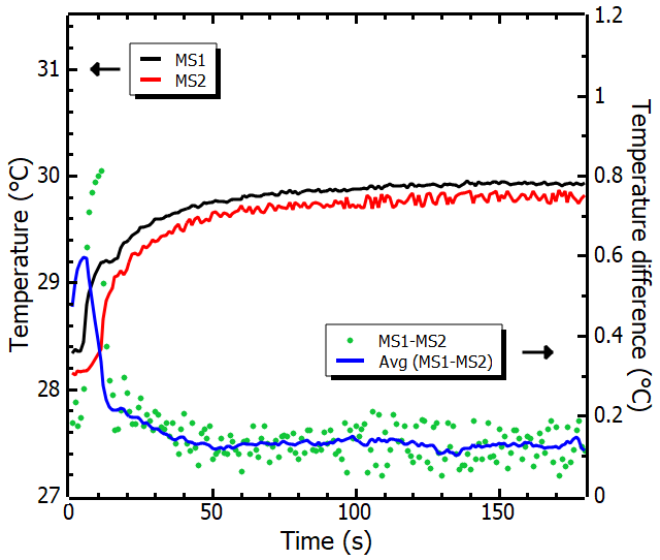

Figure 3.6 *Skin contact measurements performed on a plantar area with MS1 and MS2*

Starting from the modules MS1 and MS2 positioning, the difference recorded between them (ΔT ≈ 2.3 °C) is very close, in order of magnitude, to the value of interest indicated for DFU in the specialized medical literature. The stabilization time was about 60 seconds in this case as well (blue curve – Fig. 3.8). The method of averaging over 10 consecutive samples was employed again.

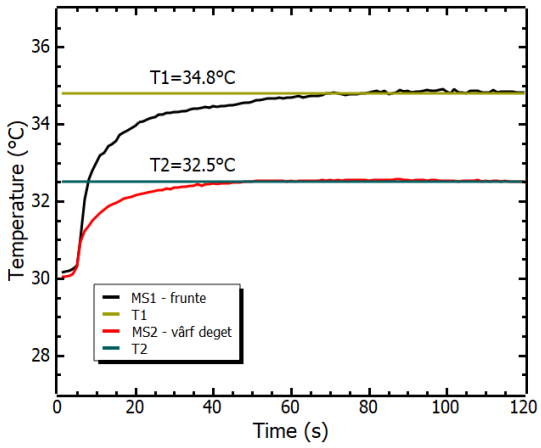

Figure 3.7 *Skin contact tests, MS1 – forehead, MS2 – index finger tip*

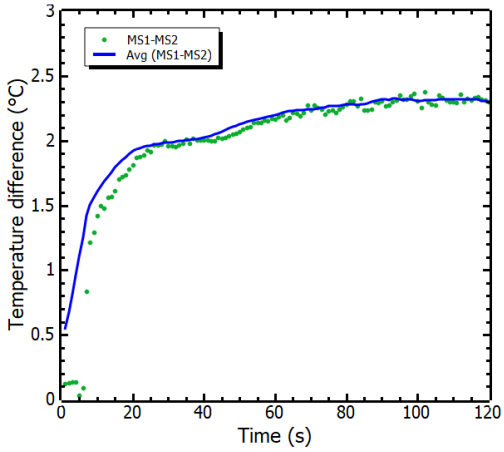

Figure 3.8 *Temperature difference recorded between MS1 and MS2*

3.5 Conclusions

In this chapter, a plantar temperature monitoring system was proposed, with potential for use in the prevention of diabetic foot ulcers. According to medical procedures, affected tissue within the plantar area can be detected by a comparative temperature analysis. The analysis targets the temperature gradient occurring either between two corresponding regions of both soles or between two distinct regions of only one. In order to functionally validate the system proposal, a prototype based on 8 modules with temperature sensors was practically implemented. The measurement resolution of 0.05 °C, the response time of about 60 seconds and an average consumption in active acquisition mode of only 17 mA were highlighted. As such, the prototype implemented for the DiaMOND architecture (Fig. 3.1) qualifies for battery supply, this being an essential feature of a portable medical system designed for measurements made in direct contact with the patient's skin. Adherence to IoT requirements, tailored for the medical field, is also ensured. It should be noted that this stage of the prototype's functional validation – previously presented – did not include tests on diabetic patients. However, the implementation considerations discussed and the results obtained provide a solid starting point for the development of a complete system, which allows simultaneous scanning of the plantar areas.

Chapter 4

Chemoresistive sensors for humidity evaluation

In this chapter, an innovative system architecture for a smart sensor is proposed, starting from a Wheatstone bridge configuration. Apart from the sensitive element itself and the signal-conditioning circuit, the proposed concept includes a power supply block, a microcontroller and a data transmission module. The conditioning circuit converts the sensor's resistive gradient into a rectangular signal with variable duty-cycle. The targeted sensing elements are chemoresistive sensors [14], [15], [42], for which base resistances vary with exposure to humidity. These sensors are based on composite nanocarbon materials, specifically oxyfluorinated carbon nano-onions (ox-CNOs-F). Starting from the theoretical analysis, two system prototypes are designed and successively implemented at the printed circuit board level to confirm the validity of the proposed operating principle.

4.1 Chemoresistive sensors based on CNO

4.1.1 Chemoresistive sensors in IoT applications

The demand for resistive sensors has increased in recent years, as they find their utility in applications such as temperature, humidity, gas concentration or mechanical strain detection. The success of this family of sensors has been determined by their simplicity and availability, aspects that can help in designing and obtaining – for a low cost – versatile readout circuits. The performance demonstrated by a resistive sensor can be equally attributed to the sensing material used and its acquisition and conditioning circuitry. Nowadays, the Internet of Things – living its finest hours – represents an important vector in the acceleration of research - development - innovation activities in the field of materials and technologies for resistive sensors. At the same time, IoT expands the range of possible applications to agriculture or the medical area, but also brings to the fore increased demands in terms of cost, miniaturization, robustness, connectivity or data protection.

Specifically, resistive sensors easily fit in greenhouse or residential air quality monitoring applications, which involve the use of dozens of such devices in a matrix of interconnected acquisition systems [4], [43]–[45]. For example, relative humidity can have a significant impact on health and the environment, being perceived as a comfort indicator. This parameter, further noted with the acronym RH and usually expressed as a percentage, represents a measure of the amount of moisture in the air relative to the maximum level of moisture that the air can retain at a certain temperature.

4.1.2 Considerations on humidity CNO sensors

At the present time, humidity has gained particular importance in the control of various processes in the chemical, pharmaceutical, wood processing, food industry, or in agriculture and in the production of integrated circuits [4], [46], [47]. For the sensors used in these applications, beyond the traditional characteristics analyzed (price, dimensions, detection mechanism, sensitivity), the sensitive material distinguishes itself as a defining performance criterion.

Nanocarbon materials (e.g., nano-onions, nano-tubes or nano-horns) and fluorinated polymer membranes have attracted the interest of the scientific community as sensitive layers for RH monitoring [48], [49], [50]. Recently, promising results in the monitoring of relative humidity obtained with oxidized Carbon nano-horns have been reported [14], [15], [42], [51]. These are hydrophilic nanomaterials with excellent conductivity and high specific surface area. In all reported situations, the measured resistance of the sensor increased proportionally to that of the RH level. In turn, Carbon nano-onions (CNO) can represent a solution for obtaining chemical sensors. This type of structure was discovered in 1992 and is presented in the form of quasi-spherical or polyhedral graphitic layers of Carbon atoms [52]. CNOs naturally have low solubility in aqueous or organic solvents due to the strong intermolecular interaction driven by van-der-Waals forces. Therefore, the chemical functionalization of this nanomaterial has been investigated, resulting in various synthesis strategies, either for adding functional chemical groups or for decorating the CNO surface with polymers [52], [53]. IMT Bucharest recently developed sensitive layers based on oxyfluorinated CNOs (ox-CNOs-F) nanocarbon materials for obtaining resistive sensors for RH [54]. The following notations were used in the doctoral thesis: **PVA** – polyvinyl alcohol, water-soluble polymer, **PVP** – polyvinylpyrrolidone, water-soluble polymer, **PL** – Plumeria Latex, **PEDOT:PSS** – poly (3,4-Ethylene-dioxytriophene) polystyrene sulfonate, conductive polymer, **IPA** – isopropyl alcohol, colorless solvent, **DMF** – dimethylformamide, colorless solvent, **IDT** – interdigital transducer. Also, the thesis describes in detail a technological process example used by IMT Bucharest to obtain the ox-CNOs-F type material, listing as well the advantages of using materials of this type [54].

4.1.3 Impedance measurements

For a better understanding of the electrical properties of chemoresistive humidity sensors, it was aimed to determine the impedance of such a structure. The doctoral thesis presents in detail the results of the frequency characterization, carried out on two sensors based on **CNO**, in a proportion of 85% [55]. The two samples differed only in the polymer added to the composition (one structure with **PVA**, the other with **PVP**). The identification parameters of the sensors are presented in Table 4.1.

Table 4.1 *Identification parameters for the CNO sensors electrically tested*

No.	Chemical compound	Dilution ratio	IDT substrate	IDT trace thickness (μm)*	Abbreviation
1	85% CNO + 15% PVA	1:100	Polyimide	25	**CNO-25-PVA**
2	85% CNO + 15% PVP	1:100	Polyimide	25	**CNO-25-PVP**

* Note: For each of the sensors listed above, the distance between IDT traces is equal to their thickness.

The test procedure used involved the application of a continuous voltage (V_{DC} of 0 V, 1 V or 2 V), over which a dynamic signal with variable amplitude and frequency was superimposed: V_{AC} of 10 mV, 50 mV and 100 mV respectively, f_{pol} between 1 kHz and 10 MHz. To model the impedance of the sample, a parallel R-C group (hereafter denoted as R_P, C_P) was chosen. Additionally, the effect of temperature on the structures was analyzed, starting from room temperature, up to 70 °C. Some of these measurements are given in Fig. 4.1. In all the cases studied in the thesis, the measurements confirmed the resistive behavior of the investigated samples. The **CNO-25-PVA** sensor (Fig. 4.1a) shows a pronounced decrease in its resistance (from 15 kΩ to 10 kΩ) when the excitation voltage V_{DC} increases up to 2 V. The three resulting resistance values remain constant until 400 kHz. Regarding the **CNO-25-PVP** structure, albeit it shows the same tendency to decrease the R_P resistance, the effect in this case takes place in a much narrower range (remaining around 2 kΩ). In contrast, the R_P resistance of the two sensors does not depend on the amplitude of the dynamic signal superimposed over V_{DC} (Fig. 4.1b). This indicates the stability these structures will have when coupled in a circuit subjected to electromagnetic radiation. Regarding the parallel capacitance (C_P) it was found that both samples register a slight decrease in this value over the entire tested frequency range. In contrast, the capacity of both sensors was shown to be very little affected by variations in the dynamic signal, V_{AC}.

For the study presented in the doctoral thesis, it was preferred to place the CNO sensors in a Wheatstone bridge type structure, polarized with constant voltage. Considerations regarding cost and broad implementation possibilities were taken into account. The utility and advantages of the Wheatstone bridge have been outlined in the thesis. It should be noted that, in the case of a resistive element inserted in such a structure, the quantity of interest at the output is the differential voltage read on the diagonal of the bridge.

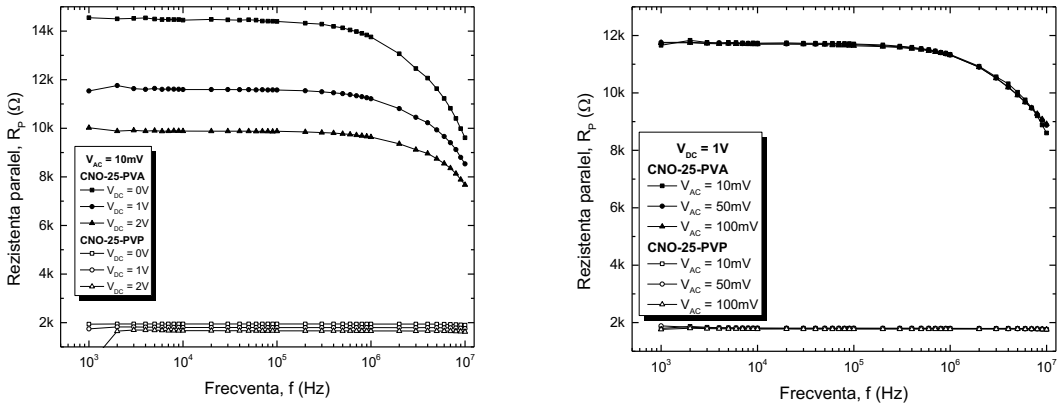

a) ***b)***

Figure 4.1 *a) R_P as a function of f_{pol} for 3 V_{DC} values; b) R_P as a function of f_{pol} for 3 V_{AC} values*

Given that experimentally obtaining four or even two perfectly paired sensitive elements might be a difficult attempt, it was decided to use the quarter-bridge configuration, with a single CNO sensor and three fixed resistors. This can lead to satisfactory output linearity, as long as sensors with moderate resistive excursions are used [13], [56], [57], [58]. The fact that the bridge itself does not offer possibilities to amplify the signal resulting from the sensor highlights the need for a conditioning block on the next stage. The amplification function is often the core of the conditioning block, because a level boost for the useful signal is essential in sensor systems that provide measurement information in a digital format. In the next sections, the proposed conditioning system for CNO sensors will be presented, with its measurement principle, practical implementation and experimental results, obtained on the model of a sensor with moderate resistive excursion (20% deviation from the nominal resistance).

4.2 CNO sensors conditioning system (CSU)

Amongst the important objectives of the doctoral thesis are the conception, design, simulation and practical implementation of a conditioning system for CNO humidity sensors, in order to integrate them into IoT ecosystems for monitoring the environment or some industrial processes. Figure 4.2 presents the block diagram of the CSU system architecture, proposed for reading CNO chemoresistive sensors. The functions of the circuit are acquisition and conditioning of the signal from the output of the actual sensor (Sensor – Fig. 4.2). In the quarter-bridge configuration shown, it can be modeled as a variable resistor, having a nominal resistance equal to R_S and a positive variation ΔR_S. For bridge swing, the value of the other three resistors is also equal to R_S. In this way, the

differential voltage on the diagonal of the bridge, depending on the bias voltage (VDD), the fixed resistance R_S and the variation ΔR_S, is given by the formula [59], [60]:

$$V_A - V_B = \frac{VDD}{2} \cdot \frac{\Delta R_S}{2 \cdot R_S + \Delta R_S} \quad (4.1).$$

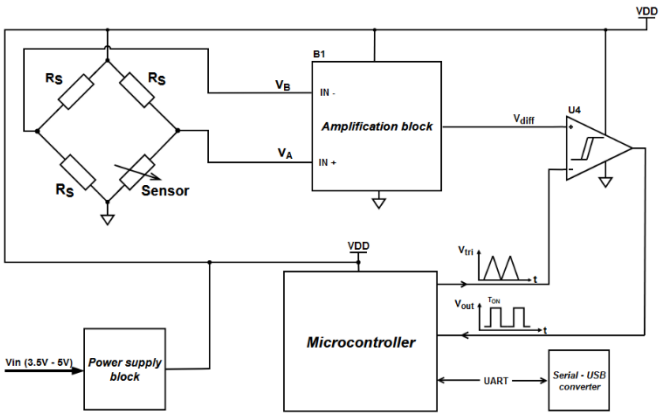

Figure 4.2 *Architecture of the signal-conditioning system proposed for CNO chemoresistive sensors*

In a simplified manner, the measurement principle of the proposed system can be described in two stages. In the first instance, an amplification is performed for the difference (V_A - V_B), with a gain factor conveniently set within the amplification block. Then, the resulting voltage is compared with a triangular signal of fixed amplitude and frequency. Thus, the microcontroller will receive a duty-cycle modulated rectangular signal, also having a fixed frequency, equal to that of the triangle. This signal will actually contain the information given by the sensor's evolution ($R_S + \Delta R_S$), through the proportionality between the duty-cycle (precisely the pulse period, T_{ON}) and its resistive gradient, ΔR_S (Sensor – Fig. 4.2). The detailed implementation of the signal amplification block, B1 is shown in Fig. 4.3. The operational amplifiers U1 and U2 are connected in a buffer configuration and serve to maintain the integrity of the differential voltage coming from the bridge, (V_A - V_B), by isolating it from the next stage.

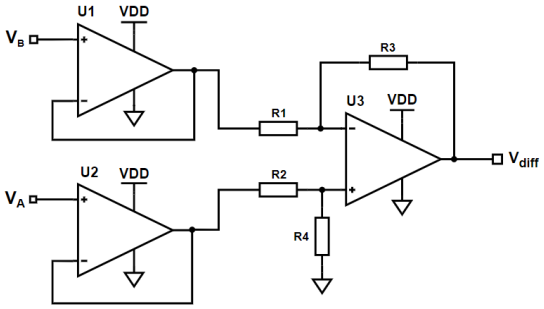

Figure 4.3 *Amplification block B1 schematic*

A key element of the circuit shown in Fig. 4.3 is the difference amplifier formed by U3, accompanied by resistors R_1 – R_4. It conveniently amplifies the voltage difference collected

from the detector bridge and, at the same time, reduces the errors introduced by the offset voltages at the inputs U1 and U2 or by the imperfect pairing of the R_S elements (Fig. 4.2). The voltage at the output of U3 (V_{diff}) can be calculated by applying the superposition theorem. As such, the finally employed relation is:

$$V_{diff} = A_d \cdot (V_A - V_B) = \frac{R_3}{R_1} \cdot (V_A - V_B) \quad (4.2).$$

This signal will be discriminated by means of a comparator (U4 - Fig. 4.2) against a triangular one, of fixed frequency (f_{tri}) and amplitude (V_{tri}), generated by the microcontroller (Fig. 4.2). This operation will determine the generation of a duty-cycle modulated rectangular signal, as a function of the resistive variation of the sensor (Sensor – Fig. 4.2). Specifically, the output of U4 will have a frequency equal to that of the triangle signal (f_{tri}) and will rise in amplitude up to the value of the comparator's supply voltage (VDD – Fig. 4.2). Therefore, the ON time of the resulting square-wave signal can be determined as a function of V_{diff}, as follows:

$$T_{ON} = T \cdot \frac{V_{diff}}{V_{tri}} \quad (4.3)$$

, where T is the period of the comparator's output signal ($1/f_{tri}$).
Finally, the dependence between the pulse width – T_{ON} and ΔR_S can be expressed, with the help of formulas (4.1), (4.2) and (4.3), as:

$$T_{ON} = k \cdot \frac{\Delta R_S}{2 \cdot R_S + \Delta R_S} \quad (4.4)$$

, where

$$k = \frac{A_d \cdot VDD \cdot T}{2 \cdot V_{tri}} \quad (4.5).$$

In relation (4.4), k represents the factor that indicates the sensitivity of the conditioning circuit (Fig. 4.3). According to relation (4.5), the its value increase can be determined only by adjusting A_d or T, since any intervention on VDD or V_{tri} can either elevate the system consumption or create instability in the operation of comparator U4. The gain of the differential amplifier (R_1 – R_4 and U3 – Fig. 4.3) indicates the smallest step ΔR_S that can be detected by the proposed CSU system.

The microcontroller (Fig. 4.2) represents an essential component in the operation of the proposed CSU system. Its contributions consist of generating the triangular signal (V_{tri}), reading the rectangular signal from the output of comparator U4 and controlling the power supply. For practical reasons, the microcontroller is powered from the same voltage source (VDD – Fig. 4.2) as the Wheatstone bridge or the amplification block B1.

4.3 CSU practical implementation

The architecture of the conditioning system shown in Fig. 4.2 was designed and parcatically implemented at printed circuit board level, using off-the-shelf components. The main blocks from the scheme were selected taking into account efficiency, consumption and dimensions as follows:

- U1, U2, U3 – OPA317 operational amplifier [61], Texas Instruments, (Fig. 4.3),
- U4 – LMV761 precision comparator [62], Texas Instruments, (Fig. 4.2),
- Microcontroller – dsPIC33CK256MP502 [63], Microchip (Fig. 4.2),
- Power supply – MCP1603 synchronous Buck converter [41], Microchip (Fig. 4.2).

In choosing the components for U1 - U3, as well as U4, the possibility of operation with asymmetric power supply, i.e., between 0 V - VDD, was taken into consideration. For the preliminary validation of the proposed conditioning principle, the model of a resistive sensor with a small swing (e.g., 20% deviation) was considered. Therefore, the variation of the sensitive element (Sensor – Fig. 4.2) was practically modeled by an ensemble consisting of a fixed resistor of 51 Ω, in series with a multi-turn potentiometer of 10 Ω (25 turns). The gain of the differential amplifier (R_1 – R_4, U3 – Fig. 4.3) was set to 10.

For comparator U4, a hysteresis window of 33 mV has been established - useful in the situation where the differential voltage (V_{diff}) applied to its inputs is very close to the offset voltage, in other words when V_{diff} takes any value close to the amplitude of the triangle, V_{tri}. Finally, Fig. 4.4 illustrates the practical realization of the CSU measurement system, showing a double-layer PCB of 6 x 4 cm^2 [60].

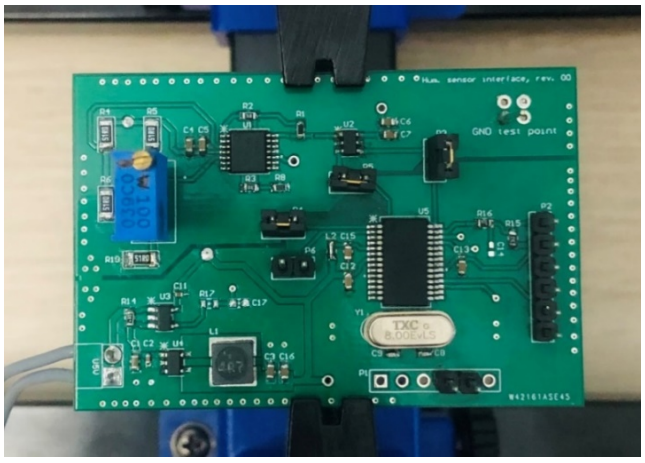

Figure 4.4 *Implemented CSU system prototype (Top Layer view)*

To demonstrate the linearity of the conditioning system with respect to the response of the sensitive element, the dependence between T_{ON} and ΔR_S was evaluated for resistive variations in the range of 51.4 Ω and 61 Ω. Beforehand, the functionality was validated through Spice simulations using the catalog features of the previously listed component

blocks as input data. It was observed that an increase in ΔR_S of only 0.4 Ω causes a pulse expansion by 23 µs, at the output of comparator U4. This resolution is essential for the correct operation of the microcontroller, located in a measurement system designed in the first instance for sensors with small resistive swings (20% increase in this case). In addition, the simulations performed confirmed the proportionality between T_{ON} and ΔR_S. The role of the microcontroller and the manner in which it is fulfilled have been extensively described in the thesis. For each turn of the potentiometer, the deviation ΔR_S was precisely measured with a GDM8341 GW Instek digital multimeter, before recording the corresponding value of T_{ON}. The experimental measurement setup was completed with a voltage source – E3642, which provided the input voltage (5 V) and with a digital oscilloscope – DSOX1204, both from Keysight Technologies. The experimental transfer characteristic of the proposed smart sensor is given in Fig. 4.5, together with the theoretical and simulation results. The proposed conditioning system demonstrated good performance, corroborated by a linearity coefficient of 99.95% (R^2_{lin}), resulting from a linear fit performed on the experimental curve, while the sensitivity was calculated at 57.71 µs/Ω. Specifically, R^2_{lin} indicates an excellent agreement between the mathematical model (relation (4.4)) and the data obtained from the measurements, reinforced by a maximum relative error of only 1.8%. The latter can be attributed to the offset voltage of the operational amplifiers (Fig. 4.3), the ripple of the VDD voltage or the inaccurate matching of the fixed elements in the bridge (R_S – Fig. 4.2).

The working principle of the conditioning system for CNO chemoresistive sensors proposed in Fig. 4.2 was theoretically analyzed, verified by simulations and experimentally validated on a prototype implemented on a PCB (Fig. 4.4).

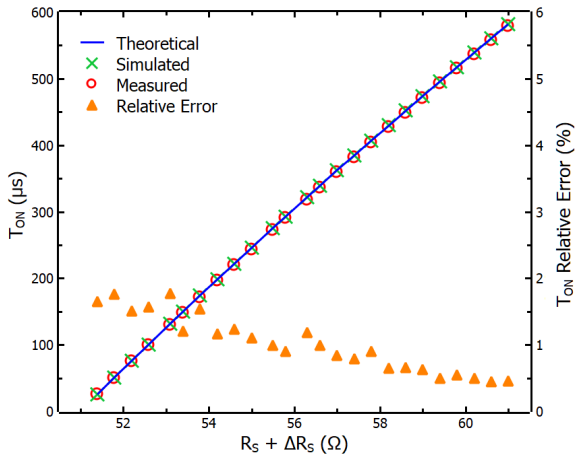

Figure 4.5 *Pulse width T_{ON} as a function of the sensitive element resistive variation: theoretical values (blue) – based on (4.3), simulated values (green), experimental values (red), relative error (orange)*

The presented implementation provides a starting point for the development of a smart sensor, aligned to IoT requirements. However, the CSU system in its current form has two major limitations. The first relates to the gain setting of the differential amplifier (U3, R_1–

R_4, Fig. 4.3). At this moment, it is necessary to modify at least two resistors (R_3, R_4 – Fig. 4.3) to obtain a new amplification factor. The second limitation refers to the existence of a single voltage range (3.3 V) for the entire system (VDD – Fig. 4.2), including the bridge bias. In the presented situation, the detector bridge together with the emulated sensor (Sensor – Fig. 4.2) determined a consumption > 50 mA. Therefore, in the following sections, an improved variant of the CSU, capable of covering a wider range of chemoresistive sensors, will be presented, starting from the same operating principle.

4.4 CSU optimization

4.4.1 Optimized CSU electrical schematic

The block diagram of the improved architecture is shown in Fig. 4.6, this graphically highlighting the most important integral blocks. The purpose of the optimizations was to increase the versatility of the proposed conditioning system and to expand the range of CNO sensors it can work with. The aim was to increase the measurement resolution and make the current consumption more efficient. Among the additions to the block diagram in Fig. 4.2 note the bridge bias control block (B1) and the adjustable gain amplification block (B2). Changes were also made to the power supplies, mainly by separating UD3V3 and UA3V3, in order to reduce costs and establish a controlled start-up sequence. In this way, the system avoids having the amplification block (B2) or the comparator U1 (Fig. 4.6) powered before the bridge is connected.

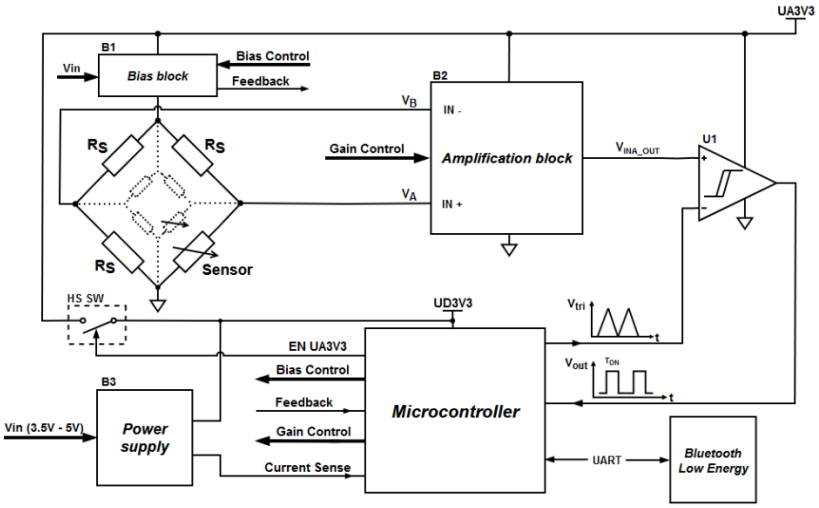

Figure 4.6 *Optimized CSU system architecture*

The quarter-bridge configuration is maintained, with the sensor still being modeled as a variable resistor, with nominal resistance equal to R_S and a positive variation ΔR_S. The

value of the other three elements also remains equal to R_S. The signal obtained at the output of comparator U1 will again contain the information taken from the sensor ($R_S + \Delta R_S$), through the proportionality between the duty-cycle (the pulse width, T_{ON}) and its resistive gradient, ΔR_S.

At the same time, Fig. 4.6 highlights the increased control that the microcontroller exerts over the analog interface in the optimized CSU system. Therefore, to manage power consumption and ensure compliance with IoT requirements, this topology includes a digitally controlled bias block (B1 – Fig. 4.6). In this regard, a control loop between the analog and digital part (microcontroller) was proposed, which ensures both the delivery of a suitable bias voltage for the bridge (decided following an a priori measurement of the CNO sensor resistance), as well as the sequential coupling of the sensitive structure to this potential. Figure 4.7 shows the bias block control mechanism in detail. The bridge bias voltage, hereafter denoted V_{BRIDGE}, is generated by means of the LDO stabilizer U2. It is directly connected to the system input voltage (Vin – Fig. 4.6) and can be activated or deactivated (via the EN V_{BRIDGE} signal) depending on the measurement protocol. For the optimized CSU version, V_{BRIDGE} can be less than or equal to UD3V3 (Fig. 4.6). At this moment, the differential voltage on the diagonal of the bridge will be calculated with the relation (4.6), similar to the previous variant (4.1), but amended by the presence of V_{BRIDGE} voltage:

$$V_A - V_B = \frac{V_{BRIDGE}}{2} \cdot \frac{\Delta R_S}{2 \cdot R_S + \Delta R_S} \quad (4.6).$$

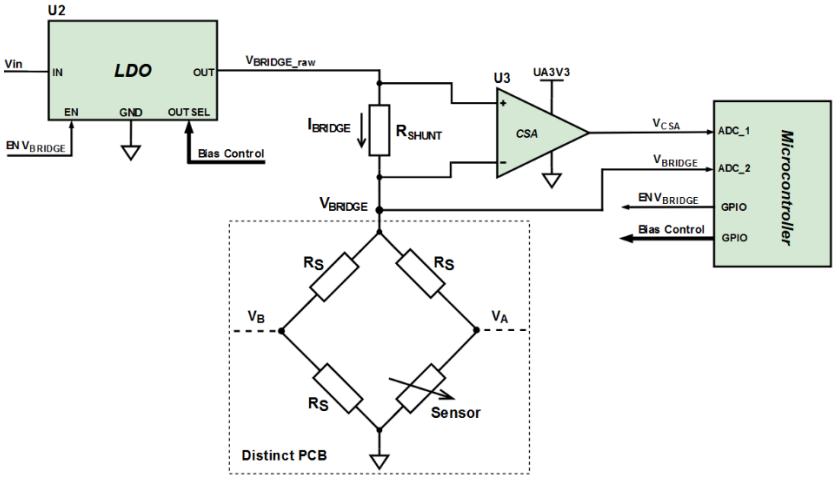

Figure 4.7 *Wheatstone bridge bias block*

The implemented circuits for UD3V3, UA3V3 and V_{BRIDGE} were analyzed in detail in the thesis. At the same time, B1 also offers the possibility to evaluate the current drawn by the bridge structure, once it is connected to the acquisition and conditioning system. This is possible thanks to the U3 amplifier. In a measurement system using the Wheatstone bridge, this can often be considered the largest current draw contributor. Thus, sending V_{CSA} to a

channel of the analog-to-digital converter (ADC) in the microcontroller, allows the system to detect when a pre-set consumption threshold for the bridge has been exceeded, which will automatically lead to the reduction of the output voltage of the U2 regulator (controlled by the **Bias Control** signal). Its complete wiring schematic has been covered in detail in the thesis. Consequently, the current required by the Wheatstone structure will be reduced. This mechanism presents advantages for the energy budget of the entire system, under the previously mentioned conditions. The configuration of block B1 (Fig. 4.7) also allows the reading of the V_{BRIDGE} bias voltage reaching the bridge after R_{SHUNT}. This facilitates then a digital compensation of the losses generated by the R_{SHUNT} series element, in order to improve the reading accuracy of the bridge differential voltage.

Next, it is proposed to use an integrated instrumentation amplifier (INA), as the central element of the block that succeeds the bridge (B2 – Fig. 4.6), thus increasing the flexibility of the amplification operation. Unlike the previous configuration (Fig. 4.3), it provides the possibility of adjusting the amplification factor for the signal coming from the detector bridge, by conveniently connecting a group of resistors to the gain terminals of the integrated circuit. In fact, both measures serve a single purpose, which is to increase the dynamic range of the system output. The way in which proportionality is ensured between the differential voltage on the diagonal of the Wheatstone bridge (V_A - V_B) and the output of the amplifier block B2 is shown in Fig. 4.8, exemplifying the possibility to obtain multiple gain values for INA, depending on the chosen measurement procedure.

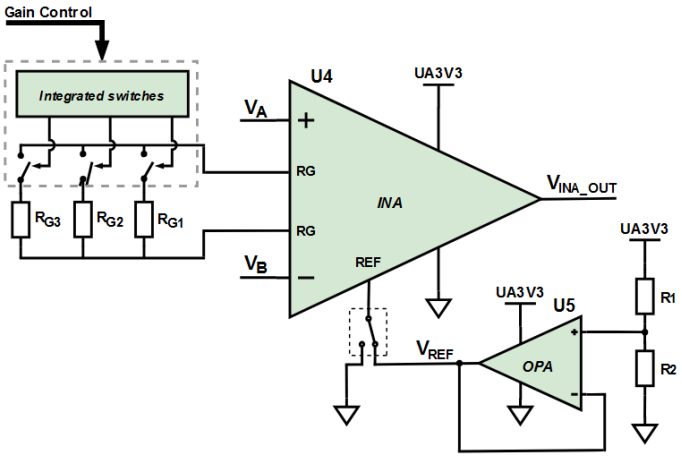

Figure 4.8 *Amplification block for the signal extracted from the Wheatstone bridge*

The **Gain Control** signal bus helps to set the gain for U4, by carrying control signals from the microcontroller that open or close the channels of 3 integrated switches. By conveniently choosing three different values for R_{G1} – R_{G3} this scheme can lead to a maximum of 7 gain values (A_d) for INA. At the same time, there is also the option for U5, together with the resistive divider of R_1 and R_2 to provide a voltage reference for U4. The presence of this voltage is particularly useful for CNO sensors with small resistive excursion (i.e., a deviation of 10% – 20% from the nominal resistance) in order to reduce

the gain values for INA. In this way, according to U5 and together with the value of the A_d factor, the voltage at the output of the instrumentation amplifier U4 is given by the formula:

$$V_{INA\_OUT} = V_{REF} + A_d \cdot (V_A - V_B) \quad (4.7).$$

The V_{INA_OUT} value obtained like this (Fig. 4.8) takes the minimum T_{ON} pulse width into a region that allows the microcontroller to read it even at a lower internal clock frequency (< 100 MHz). This fact essentially contributes to the conservation of the energy consumed by the microcontroller. The T_{ON} parameter can be further obtained using the same (4.3) relation. In the next paragraphs, the practical implementation of the optimized CSU is presented, the simulation validation of the new architecture is performed, and the experimental results obtained under laboratory conditions with different CNO sensors are presented.

4.4.2 Optimized CSU practical implementation

The CSU architecture obtained following the additions shown in Fig. 4.6 was practically translated to the PCB level with discrete components in order to evaluate its performances. The design of the main blocks of the optimized CSU system also considered the possibility to operate only with asymmetric power supply (0 V – 3.3 V). The use of a single voltage domain can qualify the proposed system for subsequent battery supply, increasing its portability. Therefore, component selection included:

- U1 – MAX9030 comparator [64], Analog Devices (Fig. 4.6),
- U2 – MAX8902A linear regulator [65], Analog Devices (Fig. 4.7),
- U3 – INA180 current amplifier [66], Texas Instruments (Fig. 4.7),
- U4 – INA317 instrumentation amplifier [67], Texas Instruments (Fig. 4.8),
- U5 – OPA317 operational amplifier [61], Texas Instruments (Fig. 4.8),
- Microcontroller – dsPIC33CK256MP502 [63], Microchip (Fig. 4.6),
- UD3V3 supply – ADP1715 linear regulator [68], Analog Devices (Fig. 4.6).

In order to evaluate the current drawn by the Wheatstone bridge, a 5 Ω shunt resistor (R_{SHUNT}) was placed in series with the V_{BRIDGE} line. To read the voltage drop on this component, the INA180 current amplifier (U3 – Fig. 4.7) was selected. For the proposed application, the R_{SHUNT} resistor was combined with the amplifier variant featuring a gain value equal to 100. In this way, the resulting circuit will be able to measure the current values consumed by bridge configurations with equivalent resistance ranging between 500 Ω and 50 kΩ. In fact, this range indicates the nominal resistances of the CNO sensors the detector bridge can be equipped with. Within the amplifier block B2, the OPA317 together with the resistive divider consisting of R_1 and R_2 is used for the option to generate the reference voltage required in certain situations for the INA317 (U4 – Fig. 4.8). An

important advantage of the amplifier block configuration (B2 – Fig. 4.8) is the flexibility in setting the gain. This is facilitated by the **Gain Control** signal bus, composed of 3 control signals coming from the microcontroller (Fig. 4.6), each one associated with an integrated switch.

In the case of the supply voltage, UD3V3 (Fig. 4.6), the use of a low-dropout type linear stabilizer (LDO) was proposed. Unlike the original CSU variant, where a synchronous buck converter was used, the LDO regulator allows to eliminate the noise introduced by the switching node of the converter. Therefore, the bridge bias voltage (V_{BRIDGE}) is also generated by an LDO (U2 – Fig. 4.7). V_{BRIDGE} is typically set to 3.3 V, but can take different values, as low as 1.8 V.

Following a thorough check of the comparator circuit used in the previous CSU version (U4 – Fig. 4.2), the presence of parasitic switching in its output signal was observed. This behavior was consistently present for various arrangements of the Wheatstone bridge (Fig. 4.2). The solution found for this problem was detailed in the PhD thesis, with the optimized CSU system variant showing "clean" transitions for both edges. The original comparator component was therefore changed to MAX9030.

Figure 4.9 shows the 3D model of the resulting printed circuit board and highlights the main building blocks of the improved architecture. It was also aimed to preserve the original dimensions of the PCB, at 6 x 4 cm^2 (Fig. 4.4). For the bridge structure, a separate PCB was made, which will be attached to connector P3, located in the upper-left part of Fig. 4.9a. To test the correct operation of the measurement system, together with a wide range of resistive sensors, this wiring was provided with sockets for the R_S positions (Fig. 4.6) and a multi-turn potentiometer placed in series with the R_S to emulate the sensitive element variation (Sensor – Fig. 4.6). Also, this is useful for CNO sensors with nominal resistance outside the usual values. The structure formed like this is illustrated in Fig. 4.10.

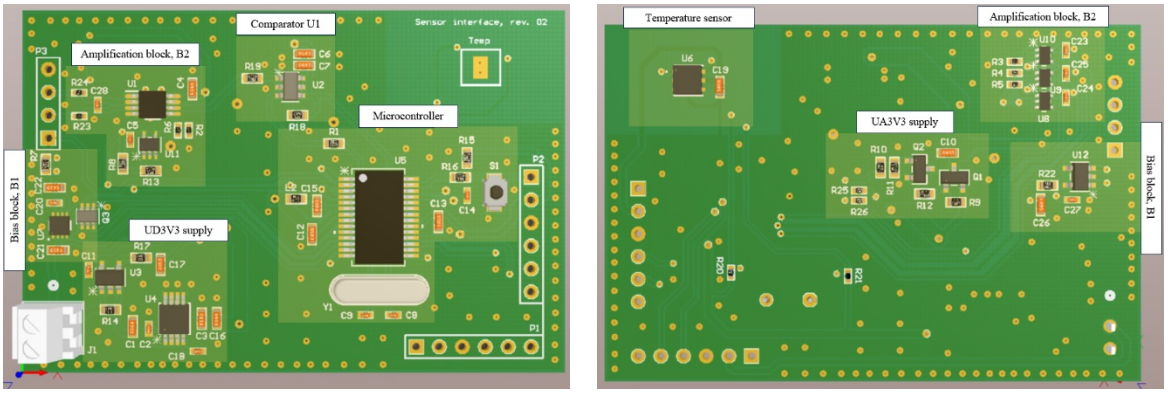

a) ***b)***

Figure 4.9 *3D model of the PCB created for the optimized CSU system: a) Top Layer view, b) Bottom Layer view*

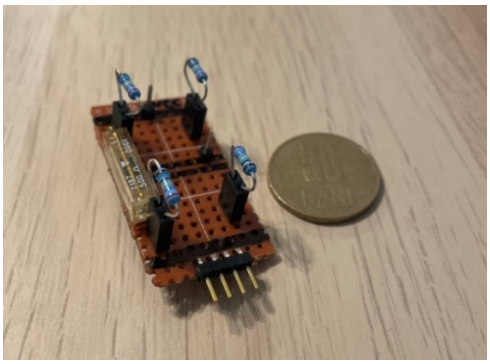

Figure 4.10 *Quarter-bridge configuration with sockets for R_S and a multi-turn trimmer for ΔR_S*

4.5 CNO sensors measurements with optimized CSU

4.5.1 Optimized CSU electrical verification

This section aims to evaluate the performance of the proposed conditioning system (Fig. 4.6) in various laboratory conditions, in order to obtain a linear dependence between its output and the sensor response. In the first instance, an electrical check of the main circuit nodes was carried out, for two different values of the sensitive element (Sensor – Fig. 4.6). Thus, the R_S positions (Fig. 4.6) were populated with resistors of 2.74 kΩ (1%) [51], and the structure that models the sensor variation was manually increased from 2.94 kΩ to 3.14 kΩ, by changing the potentiometer value by 200 Ω. The triangular signal, created by the microcontroller, had an amplitude of 2.5 V, a period equal to 1 ms and a DC component of 0 V. Similar to the measurement procedure presented in section 4.3, the R_S and ΔR_S values were precisely determined using a GDM8341 GW Instek multimeter, prior to each experimental step. The test assembly was completed with the same equipment. For these two cases, Table 4.2 presents a comparison between the T_{ON} values obtained in the cases of theoretical calculation, Spice simulation and experimental measurement.

Table 4.2 *Comparison on the T_{ON} pulse width for V_{COMP_OUT}*

$R_S + \Delta R_S$ (kΩ)	**T_{ON} pulse width of V_{COMP_OUT} (µs)**			
	Theoretical	Simulated	Measured	Deviation*
2.94	732.44	732.9	735.7	0.38%
3.14	797.8	798.06	803	0.62%

*Note: The deviation was calculated as a relative error between simulations and measurements.

The discrepancies shown through the Deviation column in Table 4.2 can be credited to the offset voltage at the input of the INA317 (U4 – Fig. 4.8), estimated in this case to be about 100 μV [67], the variations of the V_{BRIDGE} power supply and the mismatch among the R_S values (Fig. 4.6), from the Wheatstone quarter-bridge configuration. Albeit specified with a nominal resistance of 2.74 kΩ, the individually measured values for these resistors were in the range of 2.735 kΩ – 2.738 kΩ.

To achieve an experimental validation for the whole interface, i.e., *detector bridge – optimized CSU system*, under laboratory conditions, CNO chemoresistive humidity sensors, based on nanocarbon composite materials, were selected. Each one showed resistive variations in the presence of humidity – mainly in the range of 1 kΩ – 10 kΩ [14], [15], [69]. Table 4.3 shows the list of CNO humidity sensors, developed by IMT Bucharest and selected for measurements with the optimized CSU system. Structures made with **PVA** polymers were mainly chosen, except for two sensors – based on **PL**.

Table 4.3 *Identification parameters for the CNO sensors tested with optimized CSU*

No.	Chemical compound	Dilution ratio	IDT substrate	IDT trace thickness (μm)[1]	Abbreviation
1	85% PEDOT: PSS + 15% PVA	1:100	Polyimide	50	**PSS-50**
2	85% CNO + 15% PVA	1:50	Polyimide	50	**CNO-50-1**
3	33% CNO + 33% PL+ 33% SS	1:50[2]	Polyimide	50	**CNO-50-2**
4	85% CNO + 15% PVA	1:50	Polycarbonate	10	**CNO-10**
5	85% CNO + 15% PVA	1:100	Polyimide	25	**CNO-25-1**
6	85% CNO + 15% PVA	1:50	Polyimide	25	**CNO-25-2**
7	85% CNO + 15% PVA	1:50	Polyimide	25	**CNO-25-3**
8	50% CNO + 50% PL	1:50[3]	Polyimide	25	**CNO-25-4**

[1] For each of the sensors listed above, the distance between IDT traces is equal to their thickness. [2] Dilution was done in a mixture of IPA (66%) and DMF (33%). [3] Dilution is done only in IPA.

Except for the positions no. 3 and 8 in Table 4.3, compound dilution is done in water. For the experiments presented in the thesis, the V_{BRIDGE} voltage was maintained at 3.3 V, given the resistive range of the selected CNO sensors (see Fig. 4.1). Different values were used for the gain factor of U4 (Fig. 4.8), depending on the sensor resistive swing. In turn, the REF terminal (Fig. 4.8) was connected to the output of U5 in certain cases, to increase the V_{INA_OUT} voltage level. Concerning data acquisition, the goal in each case was to record the T_{ON} pulse width and, in parallel, to determine the voltage drop on the R_{SENS}. The target humidity range was in most situations 10% – 80%, going up to 90% in some cases. The measurement procedure assumed a waiting time of 3 – 5 minutes to reach equilibrium at each step of the swept RH range. Also, to allow the coupling of various Wheatstone bridges to the measurement circuit, the Sensor branch (Fig. 4.10) of the bridge PCB was modeled by stringing the sensor socket with a 500 Ω multi-turn potentiometer. Figure 4.11 shows an example of a complete experimental setup, putting together all the essentials: the optimized CSU conditioning system, the bridge, the enclosure housing the CNO sensor, the external voltage source, the multimeter and the digital oscilloscope. The connection

between the sensor enclosure and the CSU acquisition and conditioning system was ensured by two conductors of 1.5 mm diameter and 40 cm in length each. Laboratory equipment that completed the experimental setups consisted of a *LeCroy WaveSurfer 3024Z* digital oscilloscope, for validating the T_{ON} reading made by the microcontroller, and a portable digital multimeter, *EXTECH EX505*, for measuring the V_A voltage, which is used for the R_{SENS} calculation.

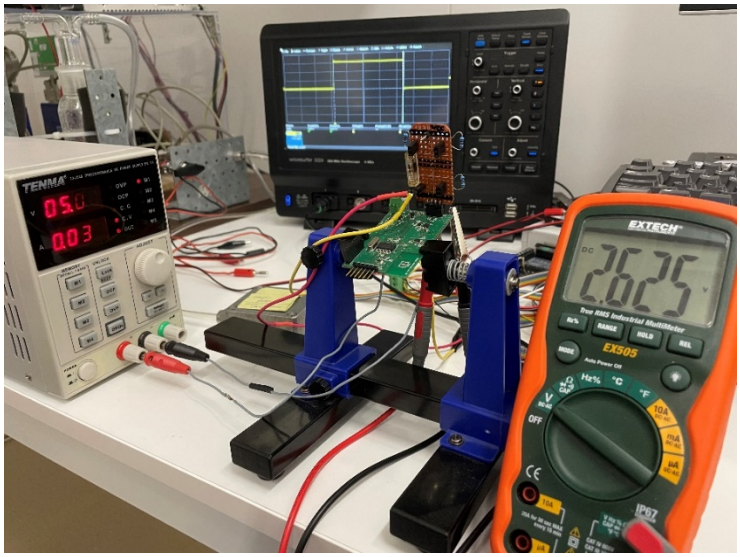

Figure 4.11 *Complete experimental setup, based on the optimized CSU prototype*

4.5.2 Humidity measurements

Figure 4.12 shows part of the variation curves – T_{ON}, R_{SENS} versus RH for the sensors listed in Table 4.3. Both details on the measurement conditions (mounting used, fixed R_S, etc.) and the performance parameters of the CSU (linearity – R^2, sensitivity) are provided.

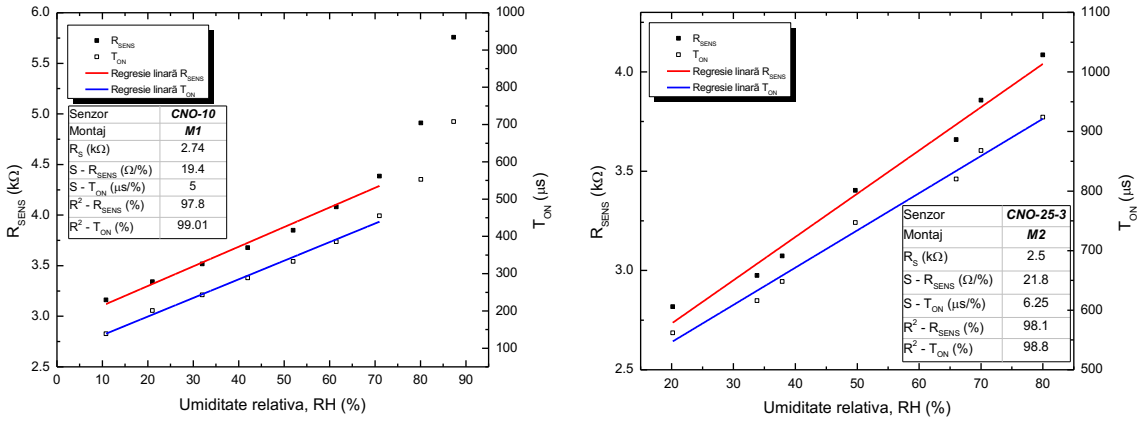

a) ***b)***

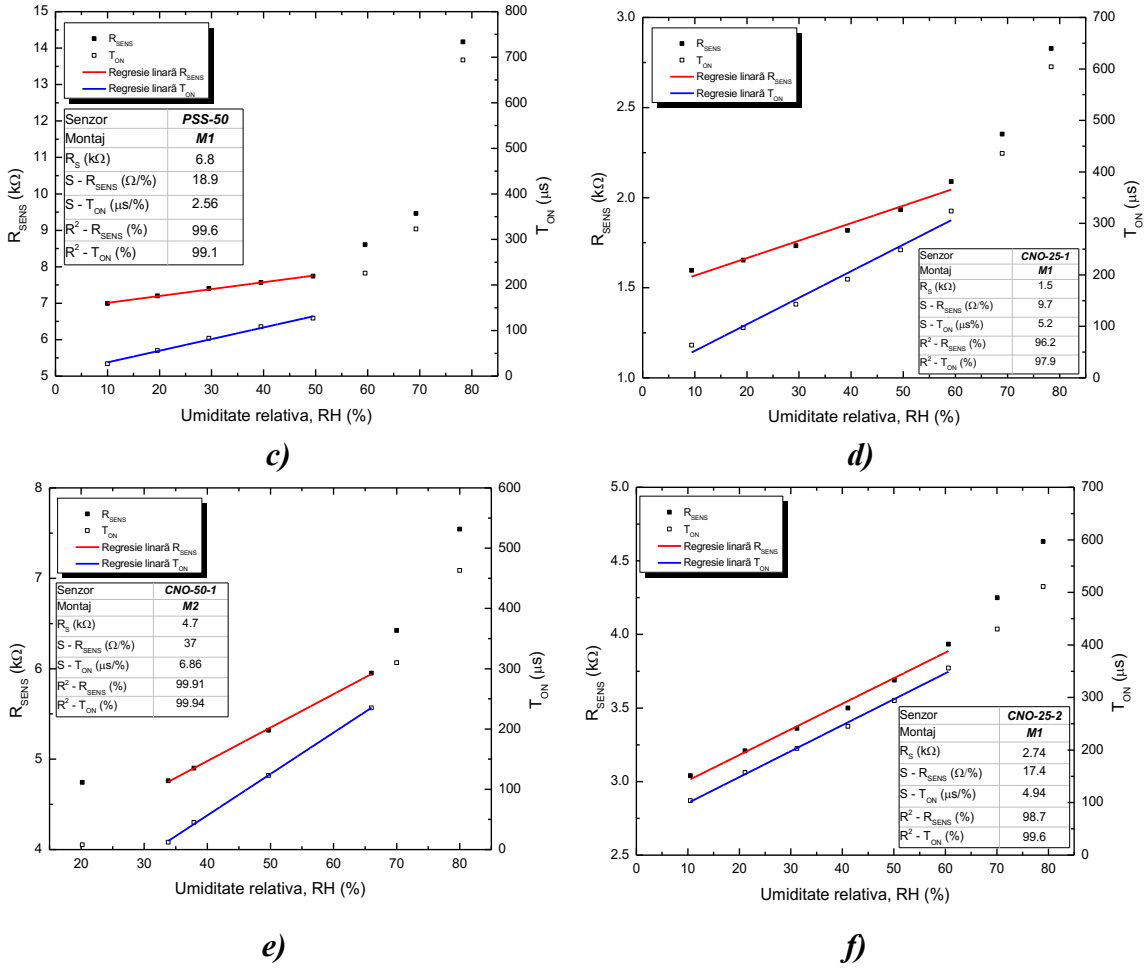

Figure 4.12 *Impulse duration on the optimized CSU output (blue) and the sensor's resistance (red) as a function of RH, for 8 different CNO samples*

In each case, the measurements confirmed the proportionality between the T_{ON} and the deviation of the sensor resistance, which occured as a result of the humidity stimulus application. Both T_{ON} and R_{SENS} increase over the entire swept RH range. Trend is mostly linear over large portions of the test range. For example, the **CNO-25-3** sensor demonstrates very good linearity over the entire measurement range (20% – 80%), both for T_{ON} and for sensor resistance (Fig. 4.12b). The **CNO-50-1** structure (Fig. 4.12e) records the highest linearity coefficient (R^2), but the range in which the sensor displays this behavior is reduced (35% – 65%). In contrast, the **CNO-10** and **CNO-25-2** sensors consistently show excellent linearity ($R^2 > 99\%$) for the T_{ON} curve between 10% and 60% (Fig. 4.12a, f). The **PSS-50** sensor follows the same trend, but on a smaller range, 10% – 50% (Fig. 4.12c). For the **CNO-25-1** structure, the linearity of the T_{ON} curve was approximated to 97.9% (Fig. 4.12d). For the portions of the RH range where the linear fit was performed, the sensitivity of the optimized CSU system was also calculated. It can be seen that the values obtained vary between 2.6 µs/% RH and 10.7 µs/% RH. Of note is the

CNO-25-3 sensor, which reveals a sensitivity of 6.25 μs/% RH, for a very good linearity over the entire tested RH interval ($R^2 \approx 99\%$, Fig. 4.12b).

The amplification factor of U4 varied depending on the excursion of the tested sensor, taking the values 2, 3 or 11 ($R_{G1} = 49.9$ kΩ, $R_{G2} = 100$ kΩ, $R_{G3} = 10$ kΩ). This confirms the versatility of the proposed conditioning system, capable of operating with a wide range of CNO sensors. In all cases, the coefficient of linearity (R^2) is higher for T_{ON}, compared to R_{SENS} (see legends of Fig. 4.12 where R^2 is given). It is therefore demonstrated that the acquisition and conditioning circuit works correctly and according to the proposed measurement principle. In addition, calibration of the *sensor – conditioning circuit system structure*, which requires a linear T_{ON} – RH variation, is feasible.

The total current consumption of the *detector bridge – conditioning system assembly* varies around 30 mA. This can be attributed to the fact that the measured CNO sensors have nominal resistances in the range of 1 kΩ – 10 kΩ, while the consumption constant contribution can be attributed to the microcontroller.

4.6 Conclusions

In this chapter, the architecture of a system for signal acquisition and conditioning from humidity sensors was presented, starting from a Wheatstone detector bridge configuration. The proposed conditioning circuit converts the sensor resistive gradient into a rectangular signal with variable duty-cycle. The targeted sensitive elements, for which the base resistance varies with exposure to humidity, were of chemoresistive type, based on oxyfluorinated carbon nano-onions materials (ox-CNOs-F). Starting from the theoretical analysis, a CSU system prototype was designed and implemented at the printed circuit board level. In the first instance, it was aimed to validate the proposed operating principle, in conjunction with a sensitive element with small resistive variation (20% deviation), in order to demonstrate a linear dependence between the sensor response and the CSU output. The experimental results led to a system transfer curve linearity coefficient of 99.95% and a sensitivity of 57.71 μs/Ω. However, limitations were observed in terms of controlling the gain factor of the block succeeding the Wheatstone bridge, as well as the current consumption. As such, a number of completions have been proposed to optimize the CSU architecture, expanding the range of CNO sensors it can work with, while also enhancing its versatility. These aspects were confirmed in various (laboratory) conditions, by means of a new prototype implemented on a printed board. Specifically, humidity measurements were made on different CNO samples, having base resistances in the range 1 kΩ – 10 kΩ and with resistive excursions between 20% and 100%. For the selected samples, the optimized variant emphasized very good linearity, over wide sections of the tested humidity range ($R^2 > 99\%$), but also satisfactory values ($R^2 = 98.8\%$) over the entire measurement RH range (20% – 80%), both for T_{ON} and the sensor's resistance.

Chapter 5

Conclusions

5.1 Obtained results

This PhD thesis was dedicated to signal acquisition and conditioning systems from temperature and humidity sensors for IoT related applications. In the conception, design and practical implementation of these systems, the goal was to follow the current demands of an IoT ecosystem. Specifically, two innovative architectures were proposed: the first, for a system for monitoring the temperature of the plantar areas, necessary to prevent the installation of diabetic foot pathology; the second, for an acquisition and conditioning system for the signal coming from chemoresistive humidity sensors, with potential for use in the evaluation of air quality in residential areas or in agriculture (equipment used inside greenhouses).

Chapter 2 of the thesis forays into the history and current significance of IoT, indicating recent application areas and outlining the identified requirements for an IoT ecosystem. It continues with the definition of an intelligent sensor system in collective acceptance and the review of two important applications – the automotive industry and the medical field. The thesis also comments on the main characteristics of a sensor along with its performance parameters. Finally, the state of the art concerning readout systems for resistive sensors was commented upon, exposed following a rigorous literature survey, among articles published in the last 5 years.

Chapter 3 was dedicated to the temperature monitoring system in the plantar area. Its main purpose – the early detection of the temperature gradient that occurs on the soles in the early stages of the establishment of diabetic foot ulcers (DFU) – was explained at length. The state of the art of temperature acquisition systems for DFU investigation was also discussed. Section 3.4 presented the architecture of the proposed system, explained its working principle and highlighted the novelty elements. Next, the practical implementation of a prototype consisting of a base plate and 8 modules with temperature sensors, which

allows the immediate scanning of a planting area, was presented in detail. Finally, the experimental results obtained with the prototype were revealed. The measuring resolution of 0.05 °C, the response time of about 60 seconds and an average consumption in active acquisition mode (1 sample/second) of 17 mA were highlighted. These aspects confirmed the intended portability of the proposed system.

Chapter 4 presented the architecture of a signal acquisition and conditioning system from humidity sensors obtained from nanocarbon composite materials. The proposed conditioning circuit converts the resistive gradient of the sensor into a rectangular signal with variable duty-cycle. Specifically, the sensitive elements targeted in the thesis consisted of chemoresistive sensors, based on oxyfluorinated carbon nano-onions (ox-CNOs-F), for which base resistances vary by exposure to humidity. *Chapter 4* was opened by humidity sensors' applications in IoT. The doctoral thesis also presented a process for obtaining ox-CNOs-F structures, made available by IMT Bucharest. The following sections were dedicated to the actual conditioning system proposed for CNO sensors. The system architecture was presented, starting from a Wheatstone quarter-bridge configuration and its working principle was exposed. Two variants were proposed – one for resistive elements with moderate swings and another one, optimized, for full excursions. The practical implementation was also discussed and the obtained experimental results were given.

5.2 Original contributions

The doctoral thesis contains a series of original contributions, disseminated through various methods throughout the PhD program. These include specialized conferences, scientific journals or research and development projects, financed from public funding. Next, the original contributions, extensively commented on in previous chapters, will be briefly presented. Punctually, each contribution will be associated with a paper published on that topic.

- Literature syntheses concerning:
  - Internet of Things exigencies and applications,
  - Particular applications for temperature and humidity sensors,
  - The use of nanocarbon materials (CNO) to obtain sensitive layers for chemoresistive sensors,
  - State of the art regarding conditioning systems for resistive sensors and temperature sensors for medical applications **[2]**, **[3]**, **[6]**.

- Architectures for IoT applications. Designed systems:
  - DiaMOND – Temperature monitoring system for the plantar areas, with applicability in preventing the installation of diabetic foot pathology **[3]**,

- CSU – System for acquiring and conditioning the signal from resistive humidity sensors, obtained from innovative nanocarbon materials **[1]**, **[2]**, **[4]**, **[6]**.

- Design of DiaMOND and CSU, with emphasis on:
  - Schematics realization and component selection **[1]**, **[2]**, **[4]**,
  - Spice simulations **[1]**, **[2]**,
  - PCB layout design for each system variant **[1]**, **[2]**, **[3]**, **[4]**.

- Parctical implementation for DiaMOND and CSU:
  - DiaMOND being composed of an acquisition main board and 8 temperature sensor modules **[3]**,
  - CSU has been realized in 2 versions:
    - ★ Variant for small resistive swings sensitive elements (e.g., 10% – 20%) **[1]**, **[2]**, **[6]**,
    - ★ Optimized variant, for full resistive swings **[4]**.

- Experimental validation for both system, by:
  - Ambient and skin temperature measurements made with the DiaMOND prototype, highlighting measurement resolution, response time and current consumption **[3]**,
  - Humidity measurements with CNO sensors, using the optimized CSU variant, tracking linearity, sensitivity and current consumption **[4]**.

Worth mentioning is the participation in the project entitled „NANO-CARBON BASED RESISTIVE SENSORS FOR IOT APPLICATIONS – FROM MATERIAL SYNTHESIS TO VERSATILE READOUT CIRCUITRY", identified as *PN-III-P2-2.1-PED-2021-4158*, *673PED from 21/06/2022*. The PhD student, as a member of the project's team, actively brought his contribution to the achievement of the project goals related to resistive sensors testing and IoT readout circuit development. He took part in drafting the project proposal and progress reports. Also, he co-authored part of the reported scientific papers. The PhD student participated in several other research grants, as well.

5.3 List of original papers published

In this section, the articles published during doctoral studies are listed with priority. In the previous paragraph, the original contributions, being the subject of each paper, were highlighted. Articles 10, 11 and patents 12, 13 were published before enrolling for PhD, but they represented an important landmark in the research topic selection.

1. **M. Serbanescu**, V.-M. Placinta, O. Buiu, G. Pristavu, F. Nastase and B. Serban, “Smart-Sensing Interface for Chemo-Resistive Sensor Based on a Wheatstone Quarter-Bridge,” in *2020 International Semiconductor Conference (CAS)*, Oct. 2020, vol. 2020-Oct., pp. 77–80, doi: 10.1109/CAS50358.2020.9268006.
2. **M. Serbanescu**, V.-M. Placinta, F. Nastase, G. Pristavu, O. Buiu, G. Brezeanu and B. Serban, “A Standalone System for Resistive Smart Sensors Based on a Wheatstone Quarter-Bridge,” *Rom. J. Inf. Sci. Technol.*, vol. 24, no. 2, pp. 222–232, 2021, WOS Q1.
3. **M. Serbanescu**, F. Nastase, F. Draghici, G. Pristavu, E. Catrina, R. Chiriac and G. Brezeanu, “Architecture for a Modular Temperature Detection System Used for Diabetic Foot Investigations,” *Proc. Int. Semicond. Conf. (CAS)*, vol. 2022–Oct., pp. 205–208, 2022, doi: 10.1109/CAS56377.2022.9934331.
4. **M. Serbanescu**, N. Dumbravescu, G. Pristavu, V. Avramescu, B. Serban, O. Buiu and G. Brezeanu, “Wheatstone Quarter-Bridge Based Resistive Smart Sensors for IoT Applications”, paper accepted for oral presentation on the *International Semiconductor Conference (CAS)*, 2024 edition, 9–11 Oct.
5. B. C. Serban, C. Cobianu, N. Dumbravescu, O. Buiu, M. Bumbac, C. N. Nicolescu, C. Cobianu, M. Brezeanu, C. Pachiu, **M. Serbanescu**, “Electrical percolation threshold and size effects in polyvinylpyrrolidone-oxidized single-wall carbon nanohorn nanocomposite: The impact for relative humidity resistive sensors design,” *Sensors*, vol. 21, no. 4, pp. 1–16, 2021*,* doi: 10.3390/s21041435, WOS Q2.
6. C. Pachiu, O. Simionescu, B. Serban, C. Parvulescu, R. Marinescu, N. Dumbravescu, F. Negoita, R. Popa, O. Buiu, **M. Serbanescu**, G. Pristavu and G. Brezeanu, “Design of a Chemoresistive Sensor Array for Potential Smart Agriculture Applications,” in *2023 Smart Systems Integration Conference and Exhibition (SSI)*, Mar. 2023, pp. 1–4, doi: 10.1109/SSI58917.2023.10387968.
7. R. Pascu, G. Pristavu, G. Brezeanu, F. Draghici, P. Godignon, C. Romanitan, **M. Serbanescu** and A. Tulbure, “60–700 K CTAT and PTAT Temperature Sensors with 4H-SiC Schottky Diodes,” *Sensors*, vol. 21, no. 3, p. 942, Jan. 2021, doi: 10.3390/s21030942, WOS Q2.
8. G. Pristavu, D.-T. Oneata, R. Pascu, **M. Serbanescu**, A. Enache, F. Draghici, G. Brezeanu, “Modeling forward characteristics of high temperature capable Schottky diodes – High-accuracy optimization methods –“, in *2023 International Semiconductor Conference (CAS),* Oct. 2023, vol. 2023–Oct., pp. 85-88, doi: 10.1109/CAS59036.2023.10303668.
9. G. Pristavu, G. Brezeanu, D.-T. Oneata, R. Pascu, F. Draghici, **M. Serbanescu** and A. Enache, “Lagging Thermal Annealing for Barrier Height Uniformity Evolution of Ni/4H-SiC Schottky Contacts”, *IEEE Transactions on Electron Devices*, vol. 71, issue 4, pp. 2805-2809, 2024, doi: 10.1109/TED.2024.3361397, WOS Q2.

10. **M. Serbanescu**, O. Ionescu, I. Georgescu, V. Dumitru, O. Buiu, “Studies for an optimal balancing system for Li ion batteries based on state of health assessment”, in *2016 International Semiconductor Conference (CAS),* Oct. 2016, vol. 2016–Oct., pp. 213-216, doi: 10.1109/SMICND.2016.7783089.
11. **M. Serbanescu**, V.-M. Placinta, O. E. Hutanu and C. Ravariu, “Smart, low power, wearable multi-sensor data acquisition system for environmental monitoring,” in *2017 10th International Symposium on Advanced Topics in Electrical Engineering (ATEE),* 2017, pp. 118–123, doi: 10.1109/ATEE.2017.7905059.
12. O. Ionescu, O. Buiu, I. Georgescu, V. G. Dumitru, B.-C. Serban, M. Brezeanu, **M. Serbanescu**, “Adaptive balancing for battery management”, US Patent 11,820,253 B2, Nov. 2023.
13. O. Ionescu, O. Buiu, I. Georgescu, V. G. Dumitru, B.-C. Serban, M. Brezeanu, **M. Serbanescu**, “Adaptive balancing for battery management”, EP 3 333 008 B1, Jun. 2022.

5.4 Prospects for future development

With respect to further development prospects, two main directions are considered. The first addresses the completion and optimization of the DiaMOND system, presented in *chapter 3*. In this sense, 4 important objectives were identified, listed below: the synchronization of temperature acquisition from two parallel strings of MS modules, the transition to battery supply, the development of a supporting mechanical support, integrating the main board and the 16 MS modules and testing the complete system under laboratory conditions and subsequently validating it under clinical conditions. To support these efforts, a PED project proposal has been submitted, identified as *PN-IV-P7-7.1-PED-2024-1060* and entitled *"MODULAR TEMPERATURE MAPPING DIGITAL SYSTEM FOR DIABETIC FOOT MONITORING"*. At the time of the doctoral thesis drafting, the proposal is in the evaluation phase.

The second direction refers to the optimized version of the CSU conditioning system, presented in *chapter 4*. In this case, 5 major objectives were set: to extend the study to other CNO sensors families (for instance the detection of ethanol), to transition to battery supply, to improve the existing PCB layout in order to identify more miniaturization possibilities, to develop an automatic linearization mechanism, either by digital methods or by modifying the gain in the amplification block depending on the slope of the T_{ON} *versus stimulus* curve (RH, ethanol, etc.) and the continuation of the collaboration with IMT Bucharest, towards obtaining bridge structures made through microtechnology techniques, which allow for an easier integration into the CSU conditioning system.

Bibliography

[1] R. S. Raji, "Smart networks for control," *IEEE Spectr.*, vol. 31, no. 6, pp. 49–55, 1994, doi: 10.1109/6.284793.

[2] M. A. Iqbal, S. Hussain, H. Xing, and M. Imran, *Enabling the Internet of Things: Fundamentals, Design, and Applications, First Edition*. Wiley, 2021.

[3] B. Bekkai, H. Bendjenna, and I. Kitouni, "Internet of Things: A Recent Survey," *Proc. - 2021 IEEE Int. Conf. Recent Adv. Math. Informatics, ICRAMI 2021*, pp. 1–9, 2021, doi: 10.1109/ICRAMI52622.2021.9585953.

[4] S. V. Gaikwad, A. D. Vibhute, K. V. Kale, and S. C. Mehrotra, "An innovative IoT based system for precision farming," *Comput. Electron. Agric.*, vol. 187, no. September 2020, p. 106291, 2021, doi: 10.1016/j.compag.2021.106291.

[5] G. Callebaut, G. Leenders, J. Van Van Mulders, G. Ottoy, L. De De Strycker, and L. Van der Van der Perre, "The Art of Designing Remote IoT Devices—Technologies and Strategies for a Long Battery Life," *Sensors*, vol. 21, no. 3, p. 913, Jan. 2021, doi: 10.3390/s21030913.

[6] C. M. Diaz, K. K. R. Choo, and A. Zunino, "Sharpening the edge: Towards improved edge computing environment for mobile and IoT applications," *Futur. Gener. Comput. Syst.*, vol. 107, pp. 1130–1133, 2020, doi: 10.1016/j.future.2019.06.017.

[7] T. G. Stavropoulos, A. Papastergiou, L. Mpaltadoros, S. Nikolopoulos, and I. Kompatsiaris, "IoT Wearable Sensors and Devices in Elderly Care: A Literature Review," *Sensors*, vol. 20, no. 10, p. 2826, May 2020, doi: 10.3390/s20102826.

[8] LG Innotek, "Sensing Solution for Autonomous Driving Cutting-edge sensor technology is the key to achieving fully autonomous vehicles," *White Pap.*, vol. 10, [Online]. Available: https://www.lginnotek.com/solution/autoDrive.do?locale=en#.

[9] J. Guerrero-Ibáñez, S. Zeadally, and J. Contreras-Castillo, "Sensor Technologies for Intelligent Transportation Systems," *Sensors*, vol. 18, no. 4, p. 1212, Apr. 2018, doi: 10.3390/s18041212.

[10] A. K. Yetisen, J. L. Martinez-Hurtado, B. Ünal, A. Khademhosseini, and H. Butt, "Wearables in Medicine," *Adv. Mater.*, vol. 30, no. 33, pp. 1–26, Aug. 2018, doi: 10.1002/adma.201706910.

[11] K. Batko and A. Ślęzak, "The use of Big Data Analytics in healthcare," *J. Big Data*, vol. 9, no. 1, p. 3, Dec. 2022, doi: 10.1186/s40537-021-00553-4.

[12] J. Moore, S. Castellanos, S. Xu, B. Wood, H. Ren, and Z. T. H. Tse, "Applications of Wireless Power Transfer in Medicine: State-of-the-Art Reviews," *Ann. Biomed. Eng.*, vol. 47, no. 1, pp. 22–38, Jan. 2019, doi: 10.1007/s10439-018-02142-8.

[13] W. Y. Du, *Resistive, Capacitive, Inductive, and Magnetic Sensor Technologies*, 1st Ed. CRC Press, Taylor & Francis Group, 2014.

[14] B. C. Serban *et al.*, "Electrical percolation threshold and size effects in polyvinylpyrrolidone-oxidized single-wall carbon nanohorn nanocomposite: The impact for relative humidity resistive sensors design," *Sensors*, vol. 21, no. 4, pp. 1–16, 2021, doi: 10.3390/s21041435.
[15] B. C. Serban *et al.*, "Quaternary holey carbon nanohorns/sno2/zno/pvp nano-hybrid as sensing element for resistive-type humidity sensor," *Coatings*, vol. 11, no. 11, pp. 1–16, 2021, doi: 10.3390/coatings11111307.
[16] E. Gómez-Ramírez, L. A. Maeda-Nunez, L. C. Álvarez-Simón, and F. G. Flores-García, "A Highly Robust Interface Circuit for Resistive Sensors," *Electronics*, vol. 8, no. 3, p. 263, Feb. 2019, doi: 10.3390/electronics8030263.
[17] G. Choi *et al.*, "A Low-Power, Low-Noise, Resistive-Bridge Microsensor Readout Circuit with Chopper-Stabilized Recycling Folded Cascode Instrumentation Amplifier," *Appl. Sci.*, vol. 11, no. 17, p. 7982, Aug. 2021, doi: 10.3390/app11177982.
[18] A. Rezvanitabar, G. Jung, Y. S. Yaras, F. L. Degertekin, and M. Ghovanloo, "A Power-Efficient Bridge Readout Circuit for Implantable, Wearable, and IoT Applications," *IEEE Sens. J.*, vol. 20, no. 17, pp. 9955–9962, 2020, doi: 10.1109/JSEN.2020.2992476.
[19] K. Elangovan, A. Antony, and A. Chandrika Sreekantan, "Simplified Digitizing Interface-Architectures for Three-Wire Connected Resistive Sensors: Design and Comprehensive Evaluation," *IEEE Trans. Instrum. Meas.*, vol. 71, no. c, 2022, doi: 10.1109/TIM.2021.3136176.
[20] K. Elangovan and A. C. Sreekantan, "Evaluation of New Digital Signal Conditioning Techniques for Resistive Sensors in Some Practically Relevant Scenarios," *IEEE Trans. Instrum. Meas.*, vol. 70, pp. 1–9, 2021, doi: 10.1109/TIM.2021.3084316.
[21] J. Golledge, M. Fernando, P. Lazzarini, B. Najafi, and D. G. Armstrong, "The Potential Role of Sensors, Wearables and Telehealth in the Remote Management of Diabetes-Related Foot Disease," *Sensors*, vol. 20, no. 16, p. 4527, Aug. 2020, doi: 10.3390/s20164527.
[22] B. Najafi and R. Mishra, "Harnessing Digital Health Technologies to Remotely Manage Diabetic Foot Syndrome: A Narrative Review," *Medicina (B. Aires).*, vol. 57, no. 4, p. 377, Apr. 2021, doi: 10.3390/medicina57040377.
[23] J. M. Pappachan, B. Cassidy, C. J. Fernandez, V. Chandrabalan, and M. H. Yap, "The role of artificial intelligence technology in the care of diabetic foot ulcers: the past, the present, and the future," *World J. Diabetes*, vol. 13, no. 12, pp. 1131–1139, Dec. 2022, doi: 10.4239/wjd.v13.i12.1131.
[24] M. A. Makroum, M. Adda, A. Bouzouane, and H. Ibrahim, "Machine Learning and Smart Devices for Diabetes Management: Systematic Review," *Sensors*, vol. 22, no. 5, p. 1843, Feb. 2022, doi: 10.3390/s22051843.
[25] E. Minty *et al.*, "Preventative Sensor-Based Remote Monitoring of the Diabetic Foot in Clinical Practice," *Sensors*, vol. 23, no. 15, p. 6712, Jul. 2023, doi: 10.3390/s23156712.
[26] A. Kairys, R. Pauliukiene, V. Raudonis, and J. Ceponis, "Towards Home-Based Diabetic Foot Ulcer Monitoring: A Systematic Review," *Sensors*, vol. 23, no. 7, p. 3618, Mar. 2023, doi: 10.3390/s23073618.

[27] M. Edmonds, C. Manu, and P. Vas, “The current burden of diabetic foot disease,” *J. Clin. Orthop. Trauma*, vol. 17, pp. 88–93, 2021, doi: 10.1016/j.jcot.2021.01.017.
[28] R. E. Sandrow, J. S. Torg, M. S. Lapayowker, and E. J. Resnick, “The use of thermography in the early diagnosis of neuropathic arthropathy in the feet of diabetics.,” *Clinical orthopaedics and related research*, vol. 88. pp. 31–33, 1972, doi: 10.1097/00003086-197210000-00004.
[29] D. G. Armstrong, K. Holtz-Neiderer, C. Wendel, M. J. Mohler, H. R. Kimbriel, and L. A. Lavery, “Skin Temperature Monitoring Reduces the Risk for Diabetic Foot Ulceration in High-risk Patients,” *Am. J. Med.*, vol. 120, no. 12, pp. 1042–1046, 2007, doi: 10.1016/j.amjmed.2007.06.028.
[30] A. Drăgulinescu, A.-M. Drăgulinescu, G. Zincă, D. Bucur, V. Feieș, and D.-M. Neagu, “Smart Socks and In-Shoe Systems: State-of-the-Art for Two Popular Technologies for Foot Motion Analysis, Sports, and Medical Applications,” *Sensors*, vol. 20, no. 15, p. 4316, Aug. 2020, doi: 10.3390/s20154316.
[31] C. Beach, G. Cooper, A. Weightman, E. F. Hodson-Tole, N. D. Reeves, and A. J. Casson, “Monitoring of Dynamic Plantar Foot Temperatures in Diabetes with Personalised 3D-Printed Wearables,” *Sensors*, vol. 21, no. 5, p. 1717, Mar. 2021, doi: 10.3390/s21051717.
[32] H. Srass, J. K. Ead, and D. G. Armstrong, “Adherence and the Diabetic Foot: High Tech Meets High Touch?,” *Sensors*, vol. 23, no. 15, p. 6898, Aug. 2023, doi: 10.3390/s23156898.
[33] T. Veneman, N. C. Schaper, and S. A. Bus, “The Concurrent Validity, Test–Retest Reliability and Usability of a New Foot Temperature Monitoring System for Persons with Diabetes at High Risk of Foot Ulceration,” *Sensors*, vol. 21, no. 11, p. 3645, May 2021, doi: 10.3390/s21113645.
[34] L. A. Lavery, B. J. Petersen, D. R. Linders, J. D. Bloom, G. M. Rothenberg, and D. G. Armstrong, “Unilateral remote temperature monitoring to predict future ulceration for the diabetic foot in remission,” *BMJ Open Diabetes Res. Care*, vol. 7, no. 1, p. e000696, Aug. 2019, doi: 10.1136/bmjdrc-2019-000696.
[35] I. L. Gordon *et al.*, “Accuracy of a foot temperature monitoring mat for predicting diabetic foot ulcers in patients with recent wounds or partial foot amputation,” *Diabetes Res. Clin. Pract.*, vol. 161, p. 108074, Mar. 2020, doi: 10.1016/j.diabres.2020.108074.
[36] S. G. Dabó, M. G. S. A. Brandão, T. M. de Araújo, N. M. Frota, and V. S. Veras, “Digital technologies in the prevention of diabetic foot: a review on mobile applications,” *ESTIMA, Brazilian J. Enteros. Ther.*, pp. 1–9, Jul. 2020, doi: 10.30886/estima.v18.870_IN.
[37] J. C. Moses, S. Adibi, N. Wickramasinghe, L. Nguyen, M. Angelova, and S. M. S. Islam, “Smartphone as a Disease Screening Tool: A Systematic Review,” *Sensors*, vol. 22, no. 10, p. 3787, May 2022, doi: 10.3390/s22103787.
[38] M. Faus Camarena, M. Izquierdo-Renau, I. Julian-Rochina, M. Arrébola, and M. Miralles, “Update on the Use of Infrared Thermography in the Early Detection of Diabetic Foot Complications: A Bibliographic Review,” *Sensors*, vol. 24, no. 1, p. 252, Dec. 2023, doi: 10.3390/s24010252.
[39] M. Serbanescu *et al.*, “Architecture for a Modular Temperature Detection System Used for Diabetic Foot Investigations,” *Proc. Int. Semicond. Conf. CAS*, vol. 2022-

Octob, pp. 205–208, 2022, doi: 10.1109/CAS56377.2022.9934331.
[40] Analog Devices, “Human Body Temperature Sensor,” *MAX30205 datasheet, March*, 2016, [Online]. Available: https://www.analog.com/en/products/max30205.html.
[41] Microchip, “2.0 MHz, 500 mA Synchronous Buck Regulator,” *MCP1603BL datasheet*, 2012, [Online]. Available: https://www.microchip.com/en-us/product/mcp1603.
[42] B. C. Serban *et al.*, “Oxidized carbon nanohorns as novel sensing layer for resistive humidity sensor,” *Acta Chim. Slov.*, vol. 67, no. 2, pp. 469–475, 2020, doi: 10.17344/ACSI.2019.5415.
[43] M. Serbanescu, V. M. Placinta, O. E. Hutanu, and C. Ravariu, “Smart, low power, wearable multi-sensor data acquisition system for environmental monitoring,” in *2017 10th International Symposium on Advanced Topics in Electrical Engineering (ATEE)*, 2017, pp. 118–123, doi: 10.1109/ATEE.2017.7905059.
[44] M. Haghi, A. Geissler, H. Fleischer, N. Stoll, and K. Thurow, “Ubiqsense: A Personal Wearable in Ambient Parameters Monitoring based on IoT Platform,” in *2019 International Conference on Sensing and Instrumentation in IoT Era (ISSI)*, Aug. 2019, pp. 1–6, doi: 10.1109/ISSI47111.2019.9043713.
[45] C. Pachiu *et al.*, “Design of a Chemoresistive Sensor Array for Potential Smart Agriculture Applications,” in *2023 Smart Systems Integration Conference and Exhibition (SSI)*, Mar. 2023, pp. 1–4, doi: 10.1109/SSI58917.2023.10387968.
[46] G. Callebaut, G. Leenders, J. Van Mulders, G. Ottoy, L. De Strycker, and L. Van der Perre, “The Art of Designing Remote IoT Devices—Technologies and Strategies for a Long Battery Life,” *Sensors*, vol. 21, no. 3, p. 913, Jan. 2021, doi: 10.3390/s21030913.
[47] A. Flammini and A. Depari, *Advanced interfaces for resistive sensors*. Elsevier Ltd, 2018.
[48] M. Ehsani, P. Rahimi, and Y. Joseph, “Structure–Function Relationships of Nanocarbon/Polymer Composites for Chemiresistive Sensing: A Review,” *Sensors*, vol. 21, no. 9, p. 3291, May 2021, doi: 10.3390/s21093291.
[49] Peter H. Huang, “HUMIDITY SENSING AND MEASUREMENT EMPLOYING HALOGENATED ORGANIC POLYMER MEMBRANES,” *U. S. Pat. 4,681,855*, 1987.
[50] Shakkottai et al., “POLYMER HYGROMETER FOR HARSH ENVIRONMENTS,” *U.S. Pat. 4,915,816*, 1990.
[51] C. Cobianu *et al.*, “Organic–inorganic ternary nanohybrids of single-walled carbon nanohorns for room temperature chemiresistive ethanol detection,” *Nanomaterials*, vol. 10, no. 12, pp. 1–16, 2020, doi: 10.3390/nano10122552.
[52] J. Bartelmess and S. Giordani, “Carbon nano-onions (multi-layer fullerenes): chemistry and applications,” *Beilstein J. Nanotechnol.*, vol. 5, no. 1, pp. 1980–1998, Nov. 2014, doi: 10.3762/bjnano.5.207.
[53] Kasama et al., “GAS SENSOR, GAS MEASURING SYSTEM USING THE GAS SENSOR, AND GAS DETECTION METHOD,” *EP 2 154 520 B1*, 2015, doi: WO 2008/140024.
[54] Octavian Buiu et al., “Raport științific și tehnic, faza I, proiect 673PED/2022, PN-III-P2-2.1-PED-2021-4158,” 2022.

[55] Octavian Buiu et al., “Raport științific final, faza III, proiect 673PED/2022, PN-III-P2-2.1-PED-2021-4158,” 2024.
[56] J. Fraden, “Handbook of Modern Sensors,” *Springer Int. Publ.*, 2015, doi: 10.1007/978-3-319-19303-8.
[57] Dataforth Corp., “Basic Bridge Circuits,” *Appl. Note*, vol. AN117, [Online]. Available: https://legacy.dataforth.com/catalog/pdf/an117.pdf.
[58] G. de Graaf and R. F. Wolffenbuttel, “Systematic approach for the linearization and readout of nonsymmetric impedance bridges,” *IEEE Trans. Instrum. Meas.*, vol. 55, no. 5, pp. 1566–1572, 2006, doi: 10.1109/TIM.2006.880318.
[59] M. Serbanescu, V.-M. Placinta, O. Buiu, G. Pristavu, F. Nastase, and B. Serban, “Smart-Sensing Interface for Chemo-Resistive Sensor Based on a Wheatstone Quarter-Bridge,” in *2020 International Semiconductor Conference (CAS)*, Oct. 2020, vol. 2020-Octob, pp. 77–80, doi: 10.1109/CAS50358.2020.9268006.
[60] M. Serbanescu *et al.*, “A standalone system for resistive smart sensors based on a wheatstone quarter-bridge,” *Rom. J. Inf. Sci. Technol.*, vol. 24, no. 2, pp. 222–232, 2021.
[61] Texas Instruments, “Zero-Drift, Low-Offset, Rail-to-Rail I/O Operational Amplifier,” *OPAx317 datasheet, June*, 2016, [Online]. Available: https://www.ti.com/product/OPA317.
[62] Texas Instruments, “LMV76x Low-Voltage, Precision Comparator With Push-Pull Output,” *LMV76x datasheet, Oct.*, 2015, [Online]. Available: https://www.ti.com/product/LMV761.
[63] Microchip, “28/36/48/64/80-Pin, 16-Bit Digital Signal Controllers with High-Resolution PWM and CAN Flexible Data,” *dsPIC33CK256MP502 datasheet*, 2022, [Online]. Available: https://www.microchip.com/en-us/product/dsPIC33CK256MP502.
[64] Analog Devices, “Low-Cost, Ultra-Small, Single/Dual/Quad Single-Supply Comparators,” *MAX9030, April 2019*, 2019, [Online]. Available: https://www.analog.com/en/products/max9030.html#documentation.
[65] Analog Devices, “Low-Noise 500mA LDO Regulators in a 2mm x 2mm TDFN Package,” *MAX8902A datasheet, January*, 2015, [Online]. Available: https://www.analog.com/en/products/max8902a.html.
[66] Texas Instruments, “INAx180 Low- and High-Side Voltage Output , Current-Sense Amplifiers,” *Ina. datasheet, July*, 2022, [Online]. Available: https://www.ti.com/lit/gpn/ina180.
[67] Texas Instruments, “INA317 Micro-Power (50-µA), Zero-Drift, Rail-to-Rail-Out Instrumentation Amplifier,” *Ina. datasheet, Nov.*, 2017, [Online]. Available: https://www.ti.com/product/INA317.
[68] Analog Devices, “500 mA, Low Dropout, CMOS Linear Regulator,” *ADP1715 datasheet*, 2006, [Online]. Available: https://www.analog.com/en/products/adp1715.html.
[69] N. Dumbravescu, O. Buiu, B.-C. Serban, R. Marinescu, and C. Pachiu, “Cycling testing methodology for PEDOT: PSS RH sensors, using different binders,” in *2023 International Semiconductor Conference (CAS)*, Oct. 2023, pp. 219–222, doi: 10.1109/CAS59036.2023.10303676.